INFLUENCE OF BARK-BEETLE-INDUCED TREE MORTALITY ON SLOPE EROSION IN THE SAN JUAN MOUNTAINS OF OURAY, CO, USA

A Thesis

by

CARLOS JAVIER GARCIA

Submitted to the Office of Graduate and Professional Studies of
Texas A&M University
in partial fulfillment of the requirements for the degree of

MASTER OF SCIENCE

Chair of Committee,	John R. Giardino
Committee Members,	John D. Vitek
	Kevin Gamache
Head of Department,	Michael Pope

August 2017

Major Subject: Geology

ABSTRACT

Degradation of the natural environment has resulted from the destruction by bark-beetles at various geographic locations around Earth. Presently, widespread tree mortality is occurring in the San Juan Mountains of southwestern Colorado. Methods of remote sensing for classifying mountain pine beetle-induced tree mortality have been developed, which will be applied to study the destruction of forest caused by the Douglas-fir beetle (*Dendroctonus pseudotsugae*), and fir-engraver beetles (*Scolytus ventralis*) that has been occurring in the Ouray, Colorado, area over the last several years. Infestations of bark-beetles result in wide-spread tree mortality, and the loss of vegetation can result in increased rates of surface runoff and slope erosion. This presents the problem identified: Does a causal relationship exist between the destruction of trees by bark-beetles and increased rates of surface runoff and erosion on the slopes in the Ouray, Colorado area?

The question posed was answered by accomplishing the following three objectives: 1. Determine if a link exists between rate of tree mortality and rate of erosion. 2. Model the rate of tree mortality and rate of erosion in the study area. 3. Provide a first approximation of surface runoff and sediment production rate.

Potential soil erosion, calculated by the model, ranged from ~0 Mg/ha/yr projected erosion in areas of low slope to a projected erosion value of ~2,300 Mg/ha/yr in areas with extremely steep slopes and areas of high drainage output conducive to

flowing water. The movement of materials down slope poses a potential hazard for the town of Ouray, CO, which is situated at the bottom of the valley.

Calculated changes in the normalized difference vegetation index (NDVI) from 2005 to 2016 showed a maximum negative change -0.53 and the maximum increase of 0.57 with a mean change of 0.08 and standard deviation of 0.09. A chi-squared test yielded a p-value of 0.00, allowing me to reject the null hypothesis and accept the alternative hypothesis, H_A, that NDVI changed over the course of this time series.

This study also provided a preliminary method for predicting surface runoff using an NDVI time series as a classification threshold input. Areas above 0.38 NDVI had a range of surface runoff values between -390,000,000 mm to -0.2 mm per tree within each pixel with a mean value between -146,916,924 mm and -5.2 mm and standard deviation of 12.6 mm – 83,674,617 mm. Runoff in areas below 0.38 NDVI had a range between 0.05 to 8.53 mm of runoff per tree with a mean of 2.15 mm and a standard deviation of 1.66 mm within each 900 m^2 pixel. Because of limitations, I was unable to conclude whether or not the null hypothesis can be rejected in that bark-beetle-induced tree mortality does not lead to an increase in surface runoff.

DEDICATION

This thesis is dedicated to my grandparents, Javier and Leonor, who have been the most wonderful second set of parents to me my entire life and have always encouraged me to pursue my passions and dreams. Your unwavering support has been your number one gift to me and I can never thank you enough. I may not carry the name, but know that you are always in my heart. Forever and ever.

ACKNOWLEDGEMENTS

I would like to thank my committee chair, Dr. Rick Giardino, for his support, guidance, and friendship through this entire project, as well as my committee members, Dr. Vitek, and Dr. Gamache, for their support.

To my mother, Cristina, words do not express how much love I have for you. Your love and guidance has been something I have treasured my entire life, and I can honestly say I could not have done any of this without you.

To my sister and best friend, Bianca, without you I would have never been an Aggie. Growing up being your brother has been one of the best things I could have ever asked for.

To my father, Carlos, and stepmother, Annette, without your support I would have never pushed myself out of my comfort zone and beyond my limits.

To the rest of my amazing family, this is for you.

To Hunter and April, thank you for bringing laughs and sanity to such a challenging time in my life.

Thank you, from the bottom of my heart, to all of you.

CONTRIBUTORS AND FUNDING SOURCES

This work was supported by a thesis committee consisting of chair Dr. John R. Giardino and committee members Dr. John D. Vitek and Dr. Kevin Gamache.

All work for the thesis was completed independently by the student without outside financial support.

NOMENCLATURE

A	RUSLE Equation Average Annual Soil Loss
C	RUSLE Equation cover-management factor
CSFS	Colorado State Forest Service
DEM	Digital Elevation Model
GDG	USDA Geospatial Data Gateway
GIS	Geographic Information System
GPS	Global Positioning System
gSSURGO	Griddled Soil Survey Geographic Database
ha	Hectare
in	Inch
K	RUSLE Equation soil-erodibility factor
L	RUSLE Equation slope length factor
LEDAPS	Landsat Ecosystem Disturbance Adaptive Processing System
LIDAR	Light Detection and Ranging
LS	Slope length and steepness factor
MCH	Methylcyclohexanone
Mg	Mega-gram
mm	millimeter
N	Nitrogen
NDVI	Normalized difference vegetation index

NRCS	Natural Resources Conservation Service
OLI	Landsat 8 Operational Land Imager
P	RUSLE Equation Support Practices
R	RUSLE Equation Rainfall-runoff erosivity factor
RUSLE	Revised Universal Soil Loss Equation
S	RUSLE Equation slope steepness factor
SR	Surface reflectance
TM	Landsat Thematic Mapper
USPED	Unit Stream Power Erosion and Deposition
UV	Ultraviolet
WRCC	Western Regional Climate Center

TABLE OF CONTENTS

Page

LIST OF FIGURES

Page

LIST OF TABLES

Page

CHAPTER I

INTRODUCTION

Climate warming coupled with recent severe droughts have resulted in vegetation mortality in various geographic locations around the world (Garrity et al., 2013). Tree mortality, in the broad sense, can be linked to regional carbon-dynamic changes, which in turn, can feedback into future changes in global climate (Kurz et al., 2008). From the late 20th century through the present, extensive bark-beetle outbreaks have caused accelerated tree mortality from Alaska to the southwestern United States (Hart and Veblen et al. 2014). Historically, insect-beetle-infestation outbreaks are most often aided by a positive influence on the beetle population, such as periods of warmer temperatures correlated with climate change, or by an event that decreases defenses of a tree, such as drought or pathogens (Hart et al., 2014; Fassnacht et al., 2013; Hyde et al., 2016). Increasing evidence of human actions through management has altered the interactions between insects and forests, resulting in more widespread insect outbreaks (Senf et al. 2015).

Within the Rocky Mountains of North America, estimates of forest mortality from insects and disease range from six to eleven million hectares (Hyde et al., 2015). In conifer forests of western North America, outbreaks of bark-beetles can induce relatively rapid tree mortality and associated color change in foliage from green to red, lagged shedding of foliage, bark, and branches, and eventual tree fall (Meigs et al., 2011). Forest mortality begins as scattered pockets and spreads as a nonlinear increase. Patterns

of tree mortality can vary within stands as a result of mixed species composition, tree density, and proximity of stands to one another (Hyde et al., 2015).

Across the Southern Rocky Mountains, mountain pine beetle (*Dendroctonus ponderosae*) and the spruce beetle (*Dendroctonus rufipennis*) are the two species responsible for bark-beetle-related damage. For example, the area affected by spruce beetles in Colorado expanded from 460 km^2 in 2009 to 1,960 km^2 in 2014 (Hart and Veblen, 2015). According to the Colorado State Forest Service (2015), an epidemic-level outbreak of bark-beetles near Ouray, Colorado, has been underway since 2013 and has continued to impact the susceptible trees in the area. The Douglas-fir beetle (*Dendroctonus* pseudotsugae), a close relative of the spruce and mountain pine beetles, and the fir engraver beetle (*Scolytus* ventralis) are destroying the forests in the region. Fir engraver beetles are estimated to have killed 85 percent of the White Fir (*Abies concolor*) in the Uncompahgre River Gorge around Ouray and in the Cow Creek drainage to the east (CSFS, 2016a). White fir and Douglas-fir continue to be killed by fir engraver and Douglas-fir beetles in several areas of the state in 2016, especially in Ouray county (CSFS, 2017).

Problem Statement

Wright discussed the beetle outbreak, and suggested it began several years ago with drought-stressed White Fir trees (*Abies concolor*), which has developed into an epidemic within the last three years (2016). Trees help prevent soil erosion by intercepting precipitation, slowing runoff, and holding soil in place. Studies have shown

that soil stability on steep forested slopes depends partly on the reinforcement from tree roots (O'Loughlin and Ziemer, 1982). It is also believed that rates of erosion are lower under forests than under other vegetation covers and root reinforcement is often cited as the most important forest influence maintaining soil stability (O'Loughlin and Ziemer, 1982). Tree death can trigger nonlinear increases in rate of erosion as bare soil patches become connected through coalescing networks that promote water runoff (Allen, 2007). As trees die and soil is exposed to natural erosional processes, the rate of erosion and volume of sediment transport could increase. The bark-beetle outbreak has been monitored through aerial-detection surveys conducted by the U.S. Forest Service and Colorado State Forest Service. These outbreak data will be analyzed to answer the problem statement for this research: Does a causal relationship exist between the destruction of trees by bark-beetles and increased erosion and surface runoff rates on the slopes in the Ouray, Colorado area?

Hypothesis and Objectives

The goal of this study is to determine if the destruction of trees by bark-beetles increase rates of erosion on slopes of the Ouray, Colorado, area. This assessment will be accomplished by fulfilling the following objectives:

1. Determine if a link exists between rates of tree-mortality and rates of erosion.
2. Model the rate of tree mortality and erosion in the area.
3. Provide a first approximation of surface runoff and sediment production rate.

These objectives are formulated as the following multiple-working hypotheses:

Hypothesis 1:

H_0: Bark-beetle-induced tree mortality has no effect on the rate of soil erosion.

H_A: Bark-beetle-induced tree mortality has an effect on the rate of soil erosion.

Hypothesis 2:

H_0: Bark-beetle-induced tree mortality does not lead to an increase in surface runoff.

H_A Bark-beetle-induced tree mortality can lead to an increase in surface runoff.

The methodology has been established to specifically fulfill each objective. The approach facilitates an explanation of how each method will be used to address each objective and ultimately answer the posed question. A summary flow chart of the approach is shown in Figure 1.

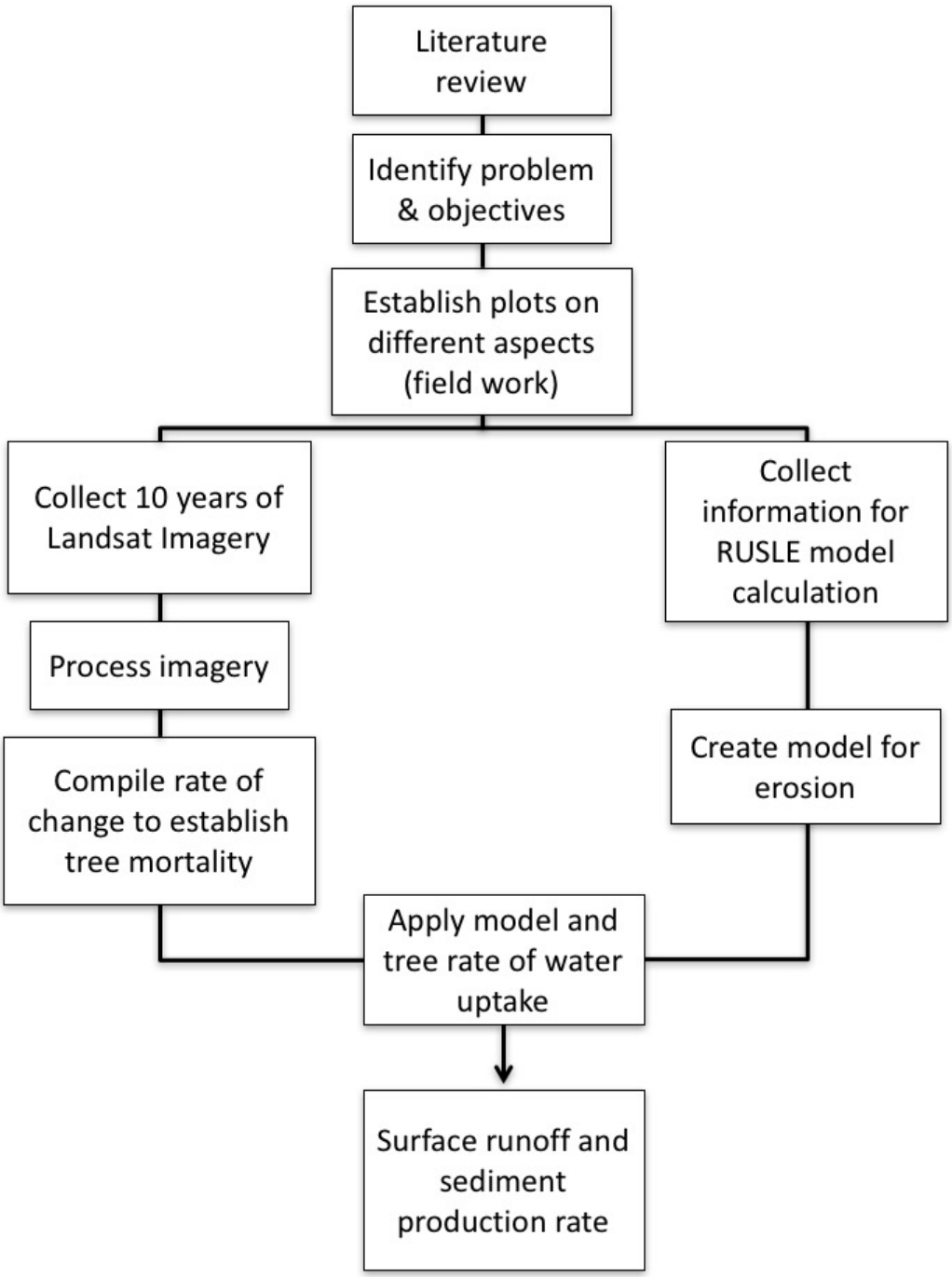

Figure 1: Flowchart illustrating order of operations to model erosion within study area.

Study Area

The study area, located within the Ouray USGS quadrangle in the town of Ouray, Colorado, which is located west of the continental divide within the San Juan Mountains (Figure 2).

Ouray, a small town in southwestern Colorado, encompasses 2.1 km^2 at an elevation of ~2,375 m. The town is located 64 km south of Montrose and 16 km northeast of Telluride. U.S. Route 550, also known as the Million Dollar Highway, provides access to the area. Several small towns are also located within the area. The Ouray Perimeter Trail, which encompasses the town provided access to field sites.

Geology and Geomorphology

Ouray, Colorado, is situated in a glaciated U-Shaped valley at an elevation of ~2,375 m. The area, underlain by expansive varieties of sedimentary, metamorphic, and igneous rocks that range in age from Proterozoic to Tertiary (Paleogene and Neogene), is capped by Quaternary glacial and surficial deposits, and Holocene deposits (Burbank and Luedke, 1981; Burbank and Luedke, 2008; Dickinson 1988). The valley is a picturesque setting with forested areas covering the lower slopes of the valley continuing up slope to the tree line.

Geologic and geomorphic processes that have sculpted the area range from glacial erosional and depositional processes, fluvial incision, volcanism, to active mass movement processes. Geologic features of the area include unconformities, incised valleys, blowouts, landslide deposits, and floodplains.

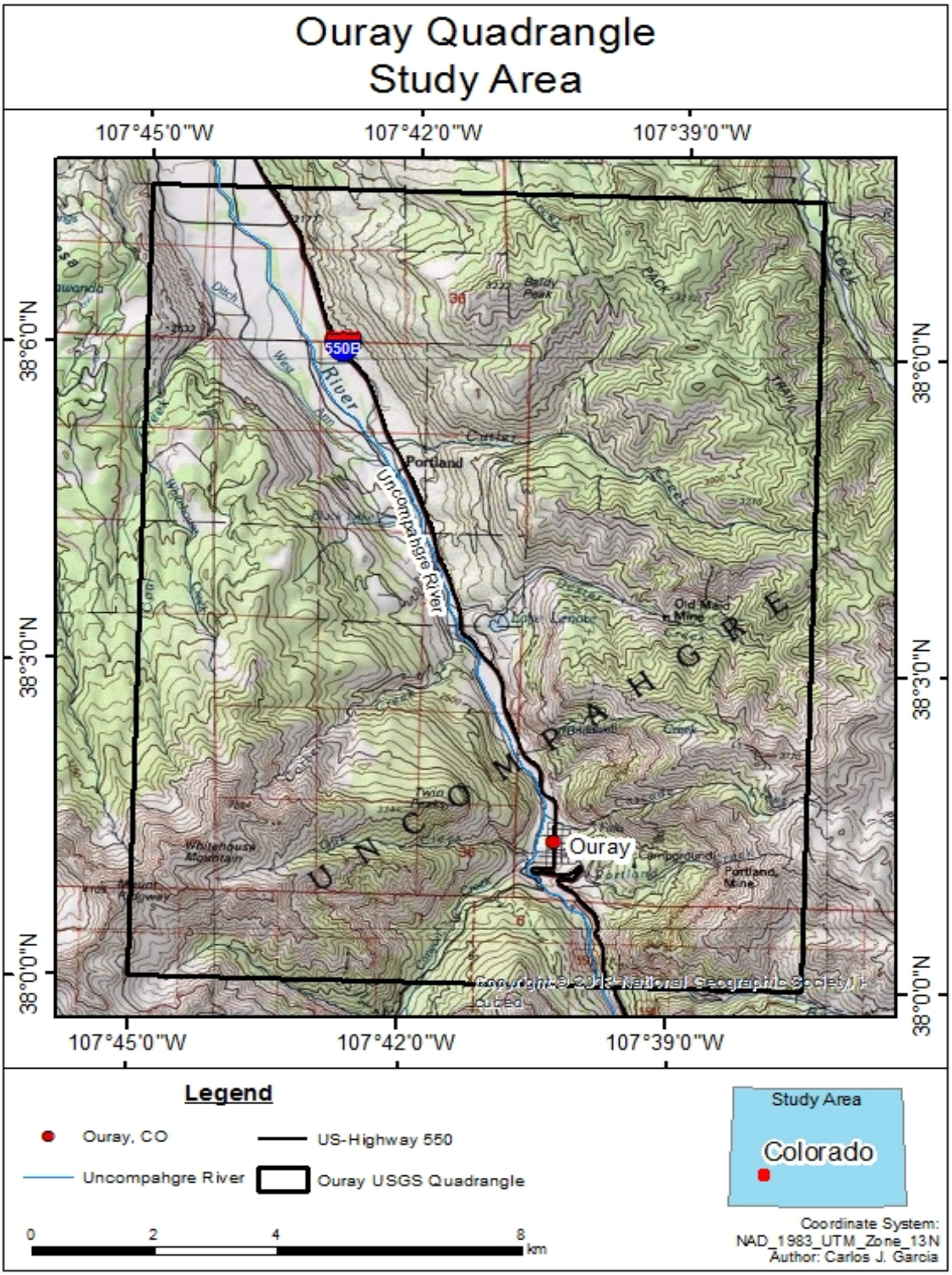

Figure 2: Extent of study area.

The Ouray Perimeter trail, a 6.75 km hiking trail that encompasses Ouray, provides scenic views of the town and the surrounding peaks (Ouray Trail Group). Several field plots were established along the Ouray Perimeter Trail. The field plots are underlain by the Uncompahgre Formation, isolated masses of glacial drift, and talus deposits, respectively (Figure 3).

The Uncompahgre Formation is metasediments of Proterozoic age, named after the Uncompahgre River Gorge south of Ouray (1,720 Ma and 1,460 Ma) (Burbank and Luedke, 2008). The formation consists of interlayered units of quartzite and slate, each several hundred meters thick, with quartzite is the dominant rock type. The quartzites are thick-to thin- bedded, strongly jointed, and white to gray or locally red or black (Burbank and Luedke, 2008). Cross-bedding, graded-bedding, and ripple marks are common. Lower contacts of the quartzites with slates are generally even and sharp whereas upper contacts with slates are commonly gradational over several meters (Moore, 2004). The slate zones are dark green, brown, and grey to black, consisting of laminated thin to thick beds that grade either into argillite or phyllite in selected places (Burbank and Luedke, 2008). The upper contact is a profound angular unconformity marking a long period of erosion (Burbank and Luedke, 2008).

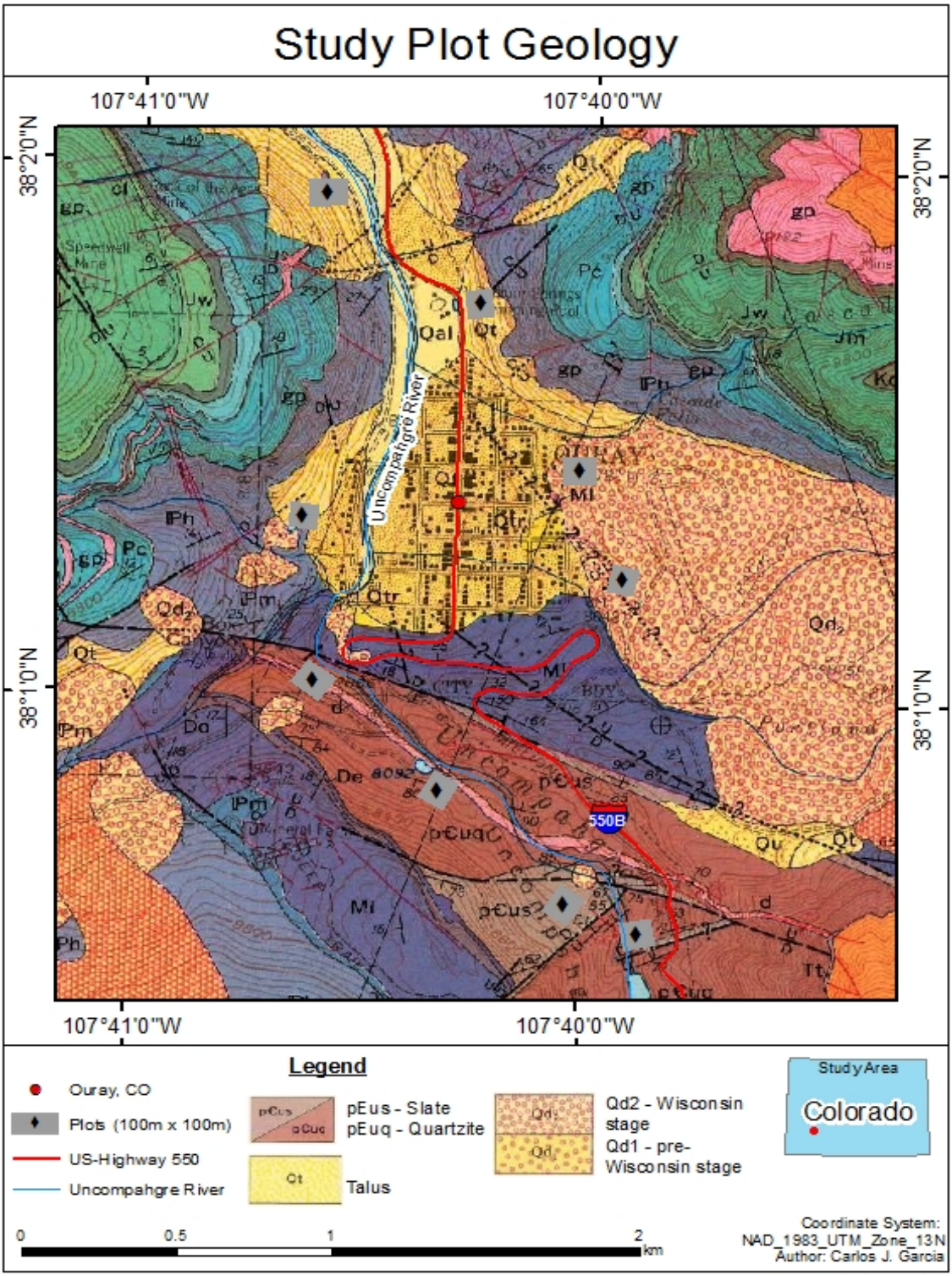

Figure 3: Field plots shown with geologic units

Pleistocene glacial drift of Wisconsin age, which is located within the Amphitheater, also underlies some of the field sites. The amphitheater is characterized by till, which is composed of unconsolidated to semi-consolidated, unsorted material ranging in size from clay to boulders and various mass movement deposits (Burbank and Luedke, 2008). The Amphitheater, which resembles a glacial cirque is interpreted to be the result of the convergence of two major glaciers where the town is now located. The mass of debris within the bowl is the result of the subsequent retreat of the glaciers, which was later subjected to slumping and sliding as well as other types of mass movements (Burbank and Luedke, 2008).

Debris flows, avalanche deposits, and talus are the most recent features, deposited in the Holocene time. This area is composed of angular rock fragments varying in size that are situated at or near the base of cliffs (Burbank and Luedke, 2008). At most locations, the talus grades into unsorted and unconsolidated colluvial deposits on flatter surfaces with increasing amounts of sand and silt (Burbank and Luedke, 2008).

Soils

The rich geologic history within the area is responsible for the development of complex soils within the area. The nine defined field plots along the Perimeter Trail are situated on various types of soils, which reflect the parent material, composition, slope, drainage, runoff, water table, and depth to the bedrock restrictive feature. Four soil associations are present in the area: Cryothents, Scout Family, Cryoboralfs, and riverwash (Figure 4).

The Cryorthents-rock outcrop complex is an extremely stony soil composed of slope alluvium derived from tuff or colluvium derived from tuff (NRCS, 2017). This soil has slopes ranging between 50 to 120 degrees, with a depth ranging from 25.4 cm to 99 cm to bedrock (NRCS, 2017). This complex is naturally well-drained with very high rates of runoff and depth to the water table greater than 203.2 cm (NRCS, 2017).

The second soil, the Scout family, is an extremely stony soil composed of slope alluvium derived from andesite, alluvium derived from andesite, or colluvium derived from andesite over till derived from andesite (NRCS, 2017). This soil has slopes ranging from 10 to 60 degrees, with more than 203.2 cm to bedrock (NRCS, 2017). This complex is naturally well-drained with high rates of runoff, and depth to the water table at more than 203.2 cm (NRCS, 2017).

The third soil, the Cryoboralfs-rock outcrop complex, is an extremely stony soil located along mountain slopes with convex profiles, typically composed of unweathered bedrock mixed with colluvium derived from mixed slope alluvium that is derived from andesite (NRCS, 2017). This soil has slopes ranging between 45 to 75 degrees, with a range between 0 and 203.2 cm to bedrock (NRCS, 2017). This complex is naturally well-drained with medium to very high rates of runoff, and depth to the water table at more than 203.2 cm (NRCS, 2017).

The final type of soil is riverwash and is found at the lowest elevations within the town of Ouray. This type of soil is found along valley floors, at slopes ranging from 0 to 4 degrees (NRCS, 2017). This complex is very poorly-drained, with runoff being

negligible (NRCS, 2017). Riverwash is frequently prone to flooding and has a depth to the water table between from 0 to 61 cm (NCRS, 2017).

Climate and Vegetation

The climate in the study area is a humid continental climate and is subject to a wide variation in temperature as the result of the topography within the region. The Ouray area experiences four distinct seasons, with short summers extending from mid-May to late June and long, but rarely severe winters (Burbank and Luedke, 2008). Based on climatological data from 1948-2006, annual average temperatures range from -9.4 °C to 28.8°C for the Ouray station (WRCC, 2006). Total mean annual precipitation and snowfall is 582.2 mm and 3,479.8 mm, respectively (Western Regional Climate Center, 2006).

The types of vegetation growth vary by location and elevation in the area and consists of scrub oak (Quercus ilicifolia), pinon (*Pinus edulis*), and juniper (*Juniperus*) on the lower slopes, whereas cottonwood (*Populus fremontii*) and willow (*Salix*) grow along the waterways, and aspen (*Populus*), pine (*Pinus*), fir (*Abies*), and spruce (*Picea*) grow on the higher mountain slopes (Burbank, W.S., and Luedke, R.G., 2008)

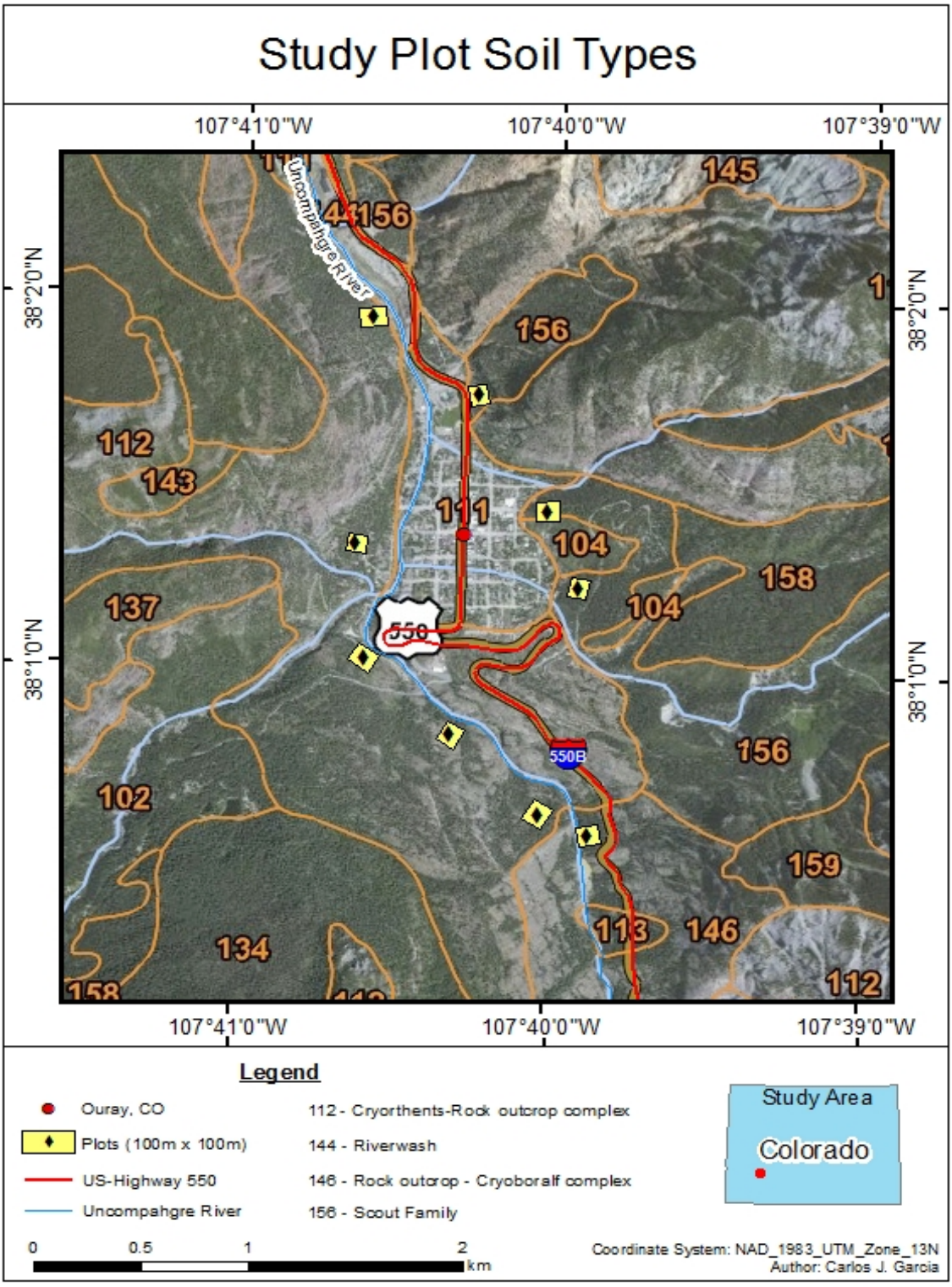

Figure 4: Field plots shown with soil classification units

CHAPTER II

MODEL OF SOIL EROSION

Introduction

Soil erosion is a major problem throughout the world that can develop into potential hazards through land degradation in mountainous environments (Das, 2016). Soil erosion is a complex natural process that depends mainly on rainfall erosivity, soil-erodibility, Land-cover, human activity, and topography (Das, 2016). Soil erosion reduces soil depth and the capacity of soils to hold water as a result of sealing and depletes plant nutrients in the soil (Das, 2016). If soil erosion is occurring at increased rates, it can have a negative impact on economic and social aspects of the environment (Gunawan et al., 2013). High rates of soil erosion can greatly impact the environment by reducing the storage capacity of a lake or reservoir, lower water quality, and remove nutrients needed by plants (Gunawan, 2013). Scientific planning for soil conservation and water management requires knowledge of the relations among the factors that cause loss of soil and water to help reduce such losses (Renard et al. 1997).

Soil erosion occurs in three phases: detachment of soil particles, transport by erosive agents such as wind and water, and deposition when sufficient erosive energy is no longer available (Gossa, 2011). Potential for soil erosion varies between watershed topography, soil characteristics, climate, land use and management practices (Gossa, 2011). Soil erosion driven by water occurs by splash erosion, sheet erosion, rill erosion, gully erosion, stream bank and river erosion, and/or mass movement.

Splash erosion occurs as a result of the impact of precipitation droplets on a soil surface and is the most important detaching agent (Morgan, 2009). The impact of raindrops on bare soil can cause soil particles to be thrown through the air over distances of several centimeters (Morgan, 2009). The continued exposure of soil to intense rainstorms can weaken the integrity of the soil considerably, breaking up the soil by mechanical and chemical weathering (Morgan, 2009).

As water continues to flow down slope, soil movement by sheet erosion can occur. This is the process of the removal of a uniform thin layer of soil by overland flow over sloping land. This type of erosion only removes a small amount of soil as water flows down slope, but its impact increases in size and severity to what is known as rill erosion (Morgan, 2009; Gossa, 2011).

Rill erosion is a coalescence of overland flow in an area with low rates of infiltration coupled with rainfall, which allows excess water to organize into a more channelized rill pattern. As water continues to move through this area with constant velocity and kinetic energy, the carrying capacity of the water increases facilitating the entrainment of soil particles, this transport results in rills further transitioning into a gully, a further concentrated and deeper form of rill erosion (Morgan, 2009; Gossa, 2011).

Stream bank erosion occurs because water flowing on the sides of the stream from overland flow into the main channel scours the banks of rivers or streams. Movement of water within river systems can also cause river erosion as rivers move sediment within the catchment area downstream (Morgan, 2009; Gossa, 2011). Each of

these types of erosion are represented in Figure 5. Continued exposure to heavy rainfall can also lead to episodes of mass movement, such as creep, slides, falls, and avalanches (Morgan, 2009).

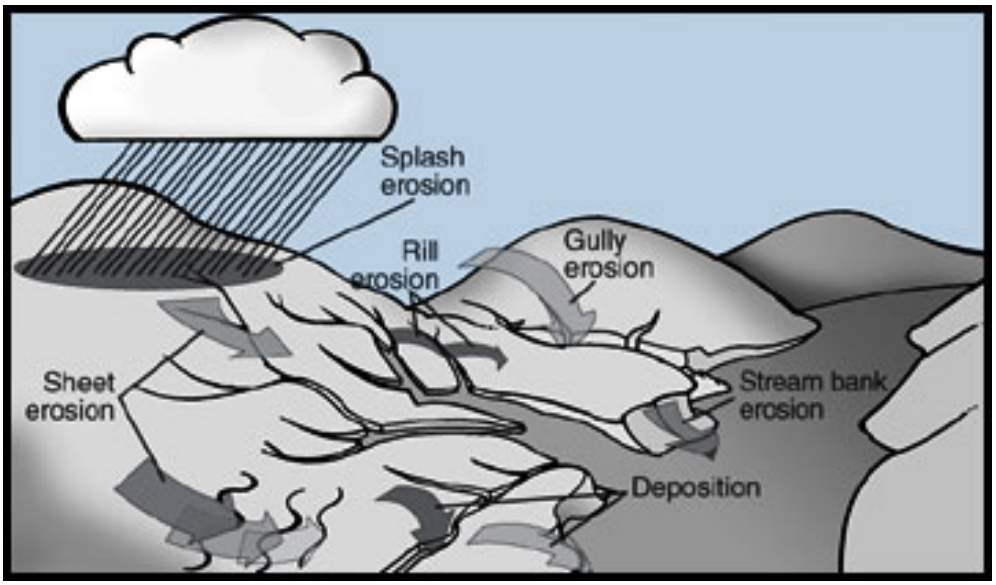

Figure 5: Types of soil erosion. Reprinted from Broz et al., 2003.

To calculate and model soil erosion, ArcGIS® and the Revised Universal Soil Loss Equation (RUSLE) equation will be utilized. This equation more accurately represents long-term averages of soil erosion compared to its predecessor, the Universal Soil Loss Equation (USLE) and is expressed as:

$$A = R \times K \times LS \times C \times P \quad (1)$$

where,
A = Average annual soil loss in Mg/ha/yr,
R = Rainfall-runoff erosivity in MJ*mm/hectare*hour,
K = Soil-erodibility factor,

LS = Slope length and steepness factor,
C = Land-cover management factor, and
P = Conservation practice factor (Renard et al., 1997).

Methods of Study

Data analysis was conducted using a guide from Kim, 2014 and a previous study from Gossa, 2011 as a model. ArcGIS® 10.3 was employed in conjunction with Microsoft Excel 2016® and information was downloaded from the USDA Natural Resources Conservation Service (NRCS) Data Gateway. Figure 6 depicts the overall workflow for determining each factor of the RUSLE equation to create an applicable soil model for the study area.

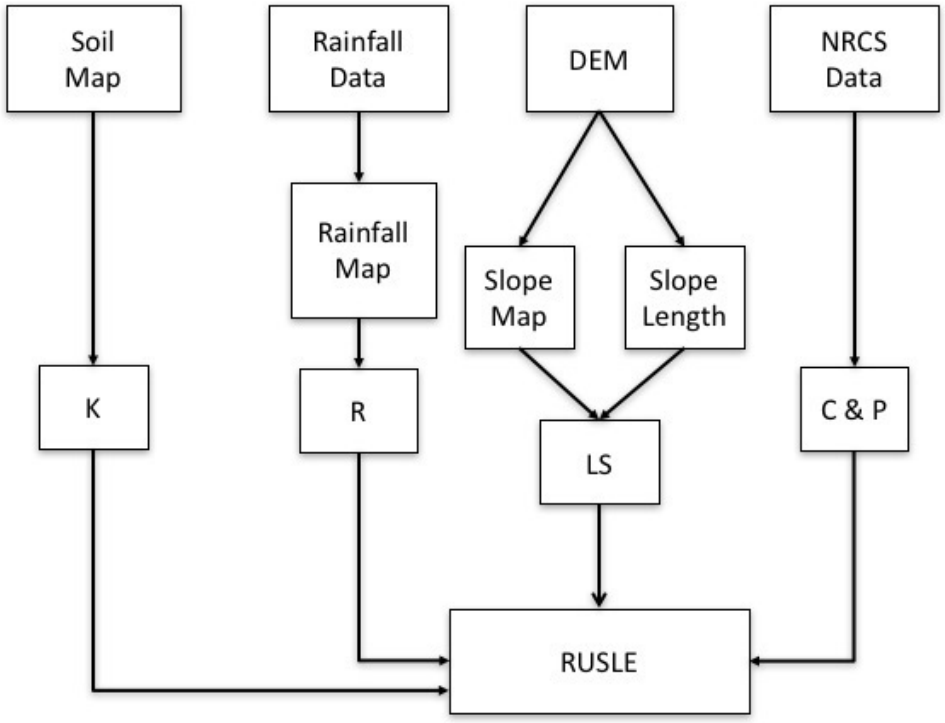

Figure 6: Methodology for generating RUSLE factors.

R-Factor

R-factor is the rainfall erosivity parameter, which is highly affected by storm intensity, duration, and potential (Kim, 2014). This study will utilize Cooper's equation, which determines the relationship between rainfall erosivity and mean annual precipitation. This equation differs from other equations because the main type of precipitation in the area is snow, which causes high precipitation (P) values and low rainfall erosivity (R) values (Cooper, 2011). Cooper's equation for the western United States is:

$$R = 9.17P^{0.20}, r^2 = 0.0176 \quad (2)$$

where,

R = Rainfall-runoff erosivity (hundred-foot-ton*inches/acre*hour), and
P = Mean annual precipitation (inches) (Cooper, 2011).

This r^2 value is extremely low, and suggests that no identifiable relationship exists between R and P (Cooper, 2011).

Precipitation information was downloaded as a shapefile containing average rainfall from 1981 – 2010 from the NRCS Data Gateway. The R-factor was then calculated by adding a new empty field of double value and using the Field Calculator tool to compute the data. Next, equation 2 was inputted into the Field Calculator along with a unit conversion factor of 0.05876 to convert English units to the metric system. The Feature to Raster tool was used isolating the calculated R-values into a raster format for continued use later in the equation.

K-Factor

The K-factor is the soil-erodibility parameter that is based on soil texture, structure, organic matter, and permeability (Kim, 2014). This data was downloaded as GIS shapefiles from the NRCS as part of the soil survey and through the ESRI online database showing Griddled Soil Survey Geographic Database (gSSURGO) survey data. These surveys included K-factors for each type of soil. Because of limitations and unreleased erodibility data in the area, however, certain areas of soils had to be interpolated using information regarding slope, soil composition, and surrounding soil-erodibility factors. The USDA will address this in at a later date when the entire soil area is fully available after being approved by USDA correlators and final review. These K-factors were then converted into raster data using the feature to raster function within GIS (Kim, 2014).

L & S-Factors

The L and S factors represent the effects of slope length (L) and slope steepness (S) on the erosion of a slope. This value was calculated using the Unit Stream Power Erosion and Deposition (USPED) method, which differs from RUSLE in that it incorporates a spatial component (Kim, 2014). A Digital Elevation Model (DEM) was downloaded from the National Elevation Dataset. This model with a 10m resolution is the basis for this factor (USGS, 2009).

The LS factor in the Revised Universal Soil Loss Equation is:

$$LS = \left(\frac{Area}{22.1}\right)^{m} * \left(\frac{\sin(t)}{0.09}\right)^{n} * (m+1) \quad (3)$$

where,

Area = area of upland flow (orientation of maximum downhill slope),
22.1 is the unit plot length;
m = slope angle variable, 0.5 for slope angles greater than 2.86° (Hickey, 2000),
t = slope in degrees,
0.09 is the slope gradient constant, and
n = flow type-dependent variable, 1.0 for areas with high spatial variability (Oliveira, et al., 2013).

The L and S factors were determined in ArcGIS® following Kim (2014):

1. Calculate flow direction from the clipped watershed DEM using the Flow Direction Tool.
2. Calculate flow accumulation with the Flow Accumulation Tool using the flow direction output data as the input raster.
3. Calculate slope of the watershed in degrees using the Slope Tool with the input being the clipped watershed DEM as the input layer.
4. Using the Raster Calculator using the LS-factor formula, given in Kim (2014) as:

$$Power(\text{“}flow\ accumulation\text{”} * [raster\ cell\ resolution]/22.1{,}0.5) *$$

$$Power(Sin(\text{“}slope\ of\ degree\text{”} * 0.01745))/0.09, 1.0) * 1.5$$

C-Factor

The C-factor of RUSLE is the land-cover management factor. This is a ratio comparing the soil loss from a specific type of vegetation cover and is used to determine the effectiveness a vegetation management system has on preventing soil loss (Kim, 2014). Land-cover data were downloaded from the USDA Geospatial Data Gateway

(GDG) as a shapefile, which was modified by adding standardized C-values for each Land-cover, as seen in Table 1 (Kim, 2014). Using the C-values within the shapefile, a conversion to raster was performed using the feature to raster function of ArcGIS® (Kim, 2014).

P-Factor

The P-factor represents the ratio of support practices that prevent soil loss. This factor is generally applied to disturbed lands and represents how surface practices such as contouring, terracing, and strip cropping are used to reduce erosion (Gossa, 2011). For areas where no support practice exists, the factor is set to 1.0 (Simms, A.D., 2003). At the time of writing, no support practice was found within the study area, so the default value of 1.0 was used.

Results

Once each of the five independent factors were calculated from the data downloaded, a simple raster calculator function within ArcGIS® was used, which provided a 10m x 10m raster of modeled output, representative of the RUSLE equation.

Average Annual Soil Loss

The resultant model, calculated from equation 1, showed most potential average annual soil loss occurring in the areas of steep slopes with ~2,300 Mg/ha/yr in potential soil erosion, which is equivalent to ~2,300 tons/ha/year, as seen in Figure 7.

Table 1: C-values for each land-cover classification (Kim, 2014).

Value	C	C-description
11	0	Open Water
21	0.003	Developed, Open Space
22	0.013	Developed, Low Intensity
23	0.2	Developed. Medium Intensity
24	0.45	Developed, High Intensity
31	1	Barren Land
41	0.003	Deciduous Forest
42	0.003	Evergreen Forest
43	0.003	Mixed Forest
52	0.009	Shrub/Scrub
71	0.013	Grassland/Herbaceous
81	0.003	Pasture/Hay
82	0.003	Cultivated Crops
90	0.001	Woody Wetlands
95	0.003	Emergent Herbaceous Wetlands

The least amount of potential soil loss occurs in areas of low slope, such as the bottom of the U-shaped valley where the previous reach of the Uncompahgre glacier occurred and has an average value of ~0 Mg/ha/year. This model had a mean of 7.72 Mg/ha/yr and a standard deviation of 29.42.

Rainfall and Runoff Erosivity (R) Factor

Rainfall and runoff, calculated using precipitation data obtained from the NRCS, were used within ArcGIS® (equation 2) as the Raster Calculator function input. This resulted in the average rainfall and runoff factor, which ranged in values from 16.16 - 19.63 hundred-foot-ton*inches/acre*hour. Using a metric unit conversion factor of 0.05876, given by Cooper, these values range from 0.95 – 1.15 MJ*mm/hectare*hour, with a mean of 1.04 and standard deviation of 0.04 (2011).

Soil-erodibility (K) Factor

Soil-erodibility was obtained through a number of resources including the NRCS soils report data online, gSSURGO data, as well as independent interpolation of any missing factors not yet released by the USDA NRCS. Input values for this parameter varied immensely with values from 0.01 to 1.0.

Slope Length and Steepness (LS) Factor

Slope length and angle were calculated using a series of methods within ArcGIS®. The LS factor was calculated using the modified version of equation 3 used in the Raster Calculator function in ArcGIS®, as given by Kim, 2014. The factor was calculated with a range between 0m - 6,654.91m with a mean of 55.95 m and standard deviation of 124.89.

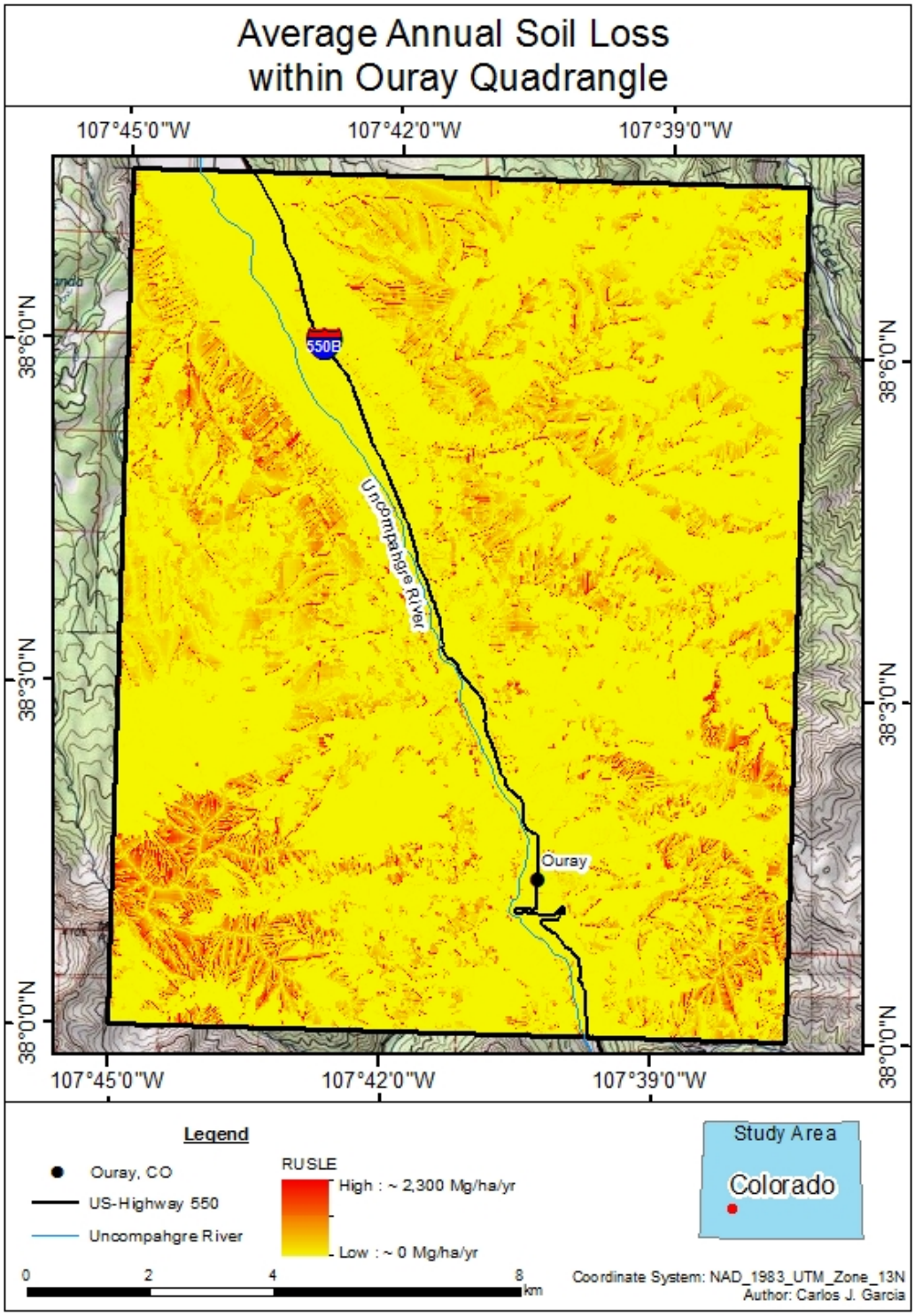

Figure 7: RUSLE model output showing average annual soil loss within the Ouray Quadrangle.

Land-cover and Support Practice (C & P) Factors

A Land-cover classification shapefile was downloaded from the USDA GDG online and was modified to include C-factors found within Kim by using the "add field" option within the attribute table (2014). This was done by adding a field and manually inputting the C-factors directly. Once this was completed, a feature to raster function was utilized in ArcGIS®, producing a raster output of solely C-factors. Each land-cover classification, represented in Table 1, are present in the study area. Literature establishing support practice factor (P-factor) were unavailable, so a default value of 1.0 was the input for the study area, which was recommended by Simms et al. (2003).

Discussion

Limitations and Improvements

The high value of ~2,300 Mg/ha/yr in potential erosion is a large calculation for the study area. This may have been caused by individual model factors or a combination of several input factors. Possibilities of questioning regarding the model can range from the DEM used to calculate slope length and angle for the L and S factors to discrepancies regarding K- and P-factors.

Weakness in the K-factor stem from the lack of complete and published information on erodibility factors within soil surveys, leading me to interpolate and assign values from the survey, which may or may not be representative of the study area as precisely as the completed survey. This weakness in soil-erodibility K-factors will be

addressed once the soil survey is completed and published for the area, which is expected at the end of 2017.

An unexpected lack of published data as well as conflicting values regarding m and n values within the LS-factor calculation can limit the application of this model. Further investigative studies regarding these values areas such as these is needed in the future, with a definitive answer to negate any doubts in this output calculation.

P-factor weakness stems from a lack of published research on support practices for the area, which would require further investigation and continued research. This area is a natural mountainous ecosystem, however, because much of the environment remains untouched by human planning interactions, which could be why no literature exists on the subject in the area.

The RUSLE model was developed to simulate soil loss at the plot level and represents maximum potential soil loss that can occur, which does not equate to sediment delivery (Simms et al., 2003). This means that this model highlights the areas of greatest susceptibility to soil loss, but actual values within the area will vary and not necessarily agree with the model. An improvement upon this model would be to couple this information with long term field soil accumulation measurements to gain a greater understanding of the overall susceptibility of soil erosion in this area.

Conclusions

This paper has shown that the RUSLE model can effectively represent the estimation of maximum possible soil loss because of erosion within the Ouray

quadrangle. R-factor was calculated to be between 0.95 – 1.15 MJ*mm/hectare*hour, and LS-Factor ranging from 0 m - 6,654.91 m. Other factors within this calculation varied spatially, with K- and C- factors between 0.01 – 1.0 and 0.00 – 1.0, respectively, depending on soil and land survey datasets.

Potential soil erosion range from ~0 Mg/ha/yr projected erosion in areas of low slope to a projected erosion value of ~2,300 Mg/ha/yr in areas with extremely steep slopes and areas of high drainage output conducive to flowing water. The movement of materials down slope poses a potential hazard for the town of Ouray, CO, which is situated at the bottom of the valley.

Caution is needed when interpreting these results because of the assumptions made to create certain parts of the model, including interpolation of soil-erodibility, K, factors. Other factors that could have affected the modeled outcome include the lack of published support practice factors for the area as well as any systemic errors within the DEM that could have attributed to errors in calculating both L and S factors, including the resampling of pixels for this calculation. With these limitations in mind and the parameter values being reassessed, this model can be used to predict the future soil erosion within the area, which is pertinent when addressing the current beetle outbreak and subsequent erosion caused by runoff from lack of tree interception.

The results of this study have provided a first approximation and a better understanding of the quantitative changes in erosion for the Ouray quadrangle using the RUSLE equation as a model. This model offers the option to quickly identify areas of high or rates of low erosion as opposed to only utilizing rates of sediment accumulation

and allows for the greater chance of determining the sources of erosion (Simms et al., 2003). This will assist in planning for any future hazards and land management within the town of Ouray and surrounding San Juan Mountains.

CHAPTER III

CHANGES IN VEGETATION AND RUNOFF CALCULATION WITHIN THE OURAY, COLORADO QUADRANGLE USING A TIME SERIES

Introduction

Drought

Droughts brought on by warmer temperatures have shown to be one of the most important global climate changes in the world. Tree mortality always accompanies warmer temperatures triggered by increasingly severe drought (Zhang et al., 2017). Warming and drought, sometimes co-occurring with insect outbreaks, have been linked to tree mortality in many regions and future changes in climate are expected to drive more extensive, severe, or frequent events of tree mortality (Anderegg et al., 2015). Droughts have recently occurred in North America, Africa, Europe, Amazonia, and Australia, with major effects on carbon sequestration, biological conservation and diversity, ecosystem function and services, climate change feedbacks, and water regulation (Anderegg et al., 2015; Zhang et al., 2017).

Insect outbreaks are often driven by drought, which stresses host trees, but also depend on many other factors including characterizations of tree stands, such as abundance, density, size, physiography, and spatial patterns across landscapes, as well as temperature and climate (Anderegg et al., 2015). This complex interaction of drought and insects may lead to increased insect populations in a forest (Anderegg et al., 2015).

Douglas-fir Beetle

The Douglas-fir beetle (*Dendroctonus pseudotsugae*) is the most destructive bark-beetle of mature Douglas-fir (*Pseudotsuga menziesii)* forests in western North America. It is a native insect found throughout the range of its only host tree, Douglas-fir, which has a range from southern Canada to northern Mexico (CSFS 2016b). These beetles have a 1-year life cycle and usually emerge mid to late spring, when the temperature is 60º F with a smaller portion emerging later in midsummer (Allen et al., 2010). Adults that attack early in the spring have the ability to reemerge for a second attack from late June to August (Allen et al., 2010). Outbreaks are usually associated with mature stands of Douglas-fir forests coupled with extended periods of below-normal precipitation (CSFS, 2016b). Female beetles construct egg galleries in the phloem layer of the tree in a distinctive vertical fashion with eggs laid in groups on alternating sides of the gallery. These eggs hatch within 1-3 weeks with new larvae mining out at right angles from the gallery (Allen et al., 2010). Once these larvae are more mature, they construct a pupal chamber at the end of the mines where they mature until emerging as adults (Allen et al., 2010). An outbreak of Douglas-fir beetles is identified by small groups of dead or dying Douglas-fir trees. Infected trees have fading needles that have changed from green to red-brown in color before starting to drop off, which occurs roughly one year after the tree has been attacked (CSFS, 2016b). Other signs include reddish-brown boring dust around the base of trees, with cracks and crevices in the bark, streaming resin along the main trunk that is white or clear in color, vertical oriented galleries underneath the bark with associated larval galleries,

woodpecker damage with bark accumulations at the base of the tree, and exit holes where adult beetles emerge from infested trees (CSFS, 2016b). Healthy Douglas-fir trees have a natural resistance to bark-beetle outbreaks; however, stresses such as wildfire, drought, and defoliation of the tops of the trees leave these trees susceptible to attack (CSFS, 2016b) (Figure 8).

Figure 8: Tree killed by Douglas-fir beetle taken 27 July, 2016.

Fir Engraver Beetle

Fir engraver beetles (*Scolytus ventralis*) are bark-beetles specialized to attack and kill true fir tree species (*Abies* spp.) and are considered the most significant bark-beetle pest of true fir forests in western North America (CSFS, 2016b). This beetle is found

from southern British Columbia, Canada south to Baja California Norte, Mexico and as far east as Montana, New Mexico, and Colorado (CSFS, 2016b). Epidemics of these beetles are associated with periods of drought (Allen et al., 2010). This species has a 1-year life cycle, with one new generation per year, except in the cooler areas of its range, where development takes two years (Allen et al., 2010). Fir engravers spend their lives within the bark and wood of host trees by feeding and developing on the inner layer of the vascular tissues of the tree (phloem) (CSFS, 2016b). An outbreak is easily spotted by the occurrence of dead or dying trees. White fir foliage usually fades from a typical blue-green color to a light orange (CSFS, 2016b). Trees infected with root disease or defoliated by Douglas-fir tussock moth or western spruce budworm are especially subject to attack (Allen et al., 2010). Infestation severity ranges from top-kill, branch dieback or the death of the entire tree (Figure 9).

Figure 9: White fir (*Abies concolor*) trees killed by fir engraver beetle. Reprinted from CSFS, 2017.

Beetle Mitigation

In an effort to prevent further expansion of the bark-beetle epidemic and reduce tree loss in the area, several management practices have been implemented by the Colorado State Forest Service (CSFS). These include thinning dense stands of trees to curb competition between trees, removing trees no later than May the year following a bark-beetle attack, using trap trees, removing wind-thrown trees, trees infected by other insects or diseases, and excess older trees, which are usually attacked first (CSFS, 2016b). Each of these practices is modified for host and pathogen.

A common cost-effective deterrent, specifically for Douglas-fir beetle management, is the use of pheromones. Pheromones are chemicals used in communication between beetles that regulate behavior of the attacking Douglas-fir beetles (CSFS, 2016b). Trees can be protected using a synthetically produced anti-aggression pheromone methylcyclohexanone (MCH), which disrupts the aggressive behavior of the beetle towards the tree (Allen et al., 2010; CSFS, 2016b). Utilizing MCH on infested trees has proven to be successful at reducing mortality, but has also failed in intense or long-lived outbreaks (Allen et al., 2010). In the case of the fir engraver beetle, no evidence exists of aggregation pheromones (Bell-Randall, 2006). The fir engraver attack dynamic is best explained by its sensitive primary attraction to its host (Bell-Randall, 2006) (Figure 10).

Figure 10: An MCH pheromone packet nailed to an uninfected Douglas-fir tree to deter beetle attack. Reprinted from CSFS, 2016b.

Sprays have also shown promise in deterring attacks, but have little effect on trees that have already fallen victim to bark-beetle attacks (CSFS, 2016a). Common sprays used in preventing beetle attacks include permethrin and carbaryl. Permethrin attack the neurological systems of insects, which paralyze them upon ingestion. Risk factors associated with Permethrin are low in terrestrial environmental impacts because it breaks down quickly when exposed to ultraviolet (UV) light, but is highly toxic to bees and extremely toxic to aquatic life (CSFS, 2016b). Carbaryl is a neurotoxin that kills insects on contact or by ingestion and persists in the environment longer than permethrin because of its higher resistance to UV light (CSFS, 2016b). This chemical carries the same risks towards bees and aquatic life, so careful and sparse utilization

must be considered when near water sources, blooming plants, and forecasted precipitation within 24 hours (CSFS 2016b).

Other various mechanical treatments include chipping wood of fallen trees and subsequently burning the slash piles, submerging cut logs in water for at least six weeks, burying logs in at least 20 cm of soil, as well as debarking the trees. These treatments are highly labor-intensive, expensive, and extremely hazardous to proceed with on the steep, remote terrain of the Colorado forest (CSFS, 2016b; Ferrell, 1996).

Beetle Impacts

The Douglas-fir and fir engraver beetles are native insects to North America and play vital parts within the ecosystem dynamics, but large outbreaks of both beetles can have intense adverse effects on the forest, which has been observed in recent times (CSFS, 2016b; CSFS, 2016b). These adverse effects include interfering with life-processes of trees, changes in nitrogen and carbon cycling in the area, changes in wildfire dynamics, and changes to hydrologic processes (CSFS, 2017; CSFS, 2016b; CSFS, 2016c; Hyde et al., 2015).

Bark-beetles disrupt two basic life-sustaining processes of the trees they infest. These two disruptions include consuming phloem tissue to build egg galleries and consuming phloem tissue as food for larvae until maturity (Hubbard et al., 2003). These two beetle interactions contribute to the disruption of photosynthate transport from the canopy to other tissues within the tree and introduce fungal spores, which germinate and

spread, preventing water conducting xylem to move water from the soil to the canopy (Hubbard et al., 2003).

According to Edburg et al., some model simulations showed strong increases in available nitrogen (N) locally because of beetle-caused tree mortality, but is unclear how the surplus moved through the larger ecosystem (2011). N concentration initially increases in the early stages of beetle infestation through detritus from falling leaves, however concentrations in N showed no change in the watersheds of Colorado impacted by bark-beetles (Griffin, J.M., et al., 2011; Rhoades et al., 2013). Findings in research show that vegetation within the watershed was utilizing this excess N available from increased litter inputs and decreased uptake by the dominant forest canopy rather than being transported out of the system downstream (Rhoades et al., 2013).

Beetle impacts on the carbon (C) cycle in conifer systems have the potential to alter the forest carbon balance, including the rate of C exchange between ecosystem and atmosphere (Hyde et al., 2015). During outbreaks, resulting widespread tree mortality reduces forest carbon uptake and increases future emissions from the decay of killed trees (Kurz et al., 2008). Contrary to this, Brown et al. reported stands with high levels or mortality became net carbon sinks within 5 years (2012). It has also been found that carbon uptake did not change as tree basal area mortality increased from 30% to 78% over three years of beetle disturbance (Reed et al., 2014). This may suggest that new and remaining vegetation plays a crucial role in the carbon cycle (Hyde et al., 2015; Reed et al., 2014). Because of these contrary studies, it could be suggested that beetle-caused

impacts to the carbon cycle are dependent upon the specific ecosystem affected (Hyde et al., 2015).

Large numbers of bark-beetle-killed trees increase the volume of fuel and the potential intensity and characteristics of wildfires (CSFS 2016b; CSFS 2016b; Hicke et al., 2012). The possibility of more extreme crown fires in beetle-killed stands will impact firefighting operations and could affect public safety (Hicke et al., 2012). Wildfires cause rapid and commonly spatially continuous change to the forest structure and in severe cases can consume all biomass and destroy soil structure (Hyde et al., 2015). Evidence is mixed, however, on the relationship between beetle-related mortality and wildfire risk (Hicke et al., 2012). The town of Ouray has implemented fuels mitigation because a wildfire could consume stabilizing vegetation and cause landslides and rock slides within its canyon walls, thereby endangering people and infrastructure of the town (CSFS, 2017).

Tree mortality results in loss of canopy cover, which directly alters evaporation, transpiration, and canopy interception and indirectly alters other watershed hydrologic processes, including infiltration, runoff, groundwater recharge, and streamflow (Adams et al., 2012). These large expanses of dead trees cannot intercept or absorb precipitation, protect the soil from erosion, and reduce soil stability, which may affect the timing of water yields and water quality (CSFS, 2016b; CSFS, 2016c). Water yields can be expected to increase following substantial loss of tree cover by die-off (Adams et al., 2012). Eroded sediment produced by the increased water yield may impair water quality and threaten aquatic habitat and human uses (Hyde et al., 2015).

Remote Sensing

Remote sensing images from satellite and aerial platforms have been valuable tools to assess extent and patterns of insect caused tree mortality (Hart and Veblen, 2015; Meddens and Hicke, 2014). With the aid of remote sensing, trees affected by bark-beetle outbreaks can be identified by the color presented when analyzing imagery. Trees that have only been infested are still green, but foliar moisture content declines in affected trees. This loss of moisture content leads to a decreased reflection in near infrared radiation (NIR) and increased reflection in shortwave infrared wavelengths (SWIR) (Hart and Veblen, 2015). As the outbreak progresses, the affected foliation of the tree turns a reddish-brown coloring, which indicates the beetles have already left the host. Remote sensing has been successfully employed to assess mortality in the red stage (Franklin et al., 2003; Coops et al., 2006; White et al., 2007), and more recently the grey stage (Meddens et al., 2011).

Previous remote studies have utilized a variety of approaches to map insect disturbances, including Moderate Resolution Imaging Spectroadiometer (MODIS), time-series data, aerial sketch mapping and photography, Hyperion, Quickbird, GeoEye-1, ASTER, SPOT, Ikonos, Rapid Eye, HyMAP, and Landsat (Lausch et al. 2013; Meigs et al. 2011). Medium- and coarse-resolution imagery, such as Landsat and MODIS, detect tree mortality at the stand/landscape scale and have wider spatial coverage (Meddens and Hicke, 2014). Landsat data can also be utilized for prediction of continuous tree mortality within a pixel as opposed to a categorical classification, which provides a more sensitive characterization of outbreak dynamics (Meigs et al., 2011).

Bark-beetle infestations have been occurring for long periods of time; however, many studies show the outbreak stages as relatively abrupt or slower processes (Kennedy et al. 2010; Meigs et al. 2011). Therefore, a multi-temporal change must be considered to establish the rate and severity of a bark-beetle outbreak. To provide a reliable analysis of bark-beetle-related effects in forests, this project will integrate a Landsat image time series (LITS) using the normalized difference vegetation index (NDVI). Previous work by Hart and Veblen identified NDVI as a useful vegetation index for distinguish between gray-stage spruce beetle outbreak and non-forest in mountain pine beetle infested areas (2015). This will be applied to study the two beetles in this study area, which are close relatives of previously studied beetles.

Methods of Study

Field Work

Before visiting the study area, extensive research was conducted on the area, including the extent of bark-beetle outbreaks within the actual town of Ouray (Figure 11). The infestation was found to span much of the town. Because of the topographic relief within the town, the Ouray Perimeter Trail was chosen as a medium to explore the affected area.

The town of Ouray, Colorado was visited for field work in July, 2016. The extent of the bark-beetle epidemic was easily seen throughout the drive through the town. Upon starting field methods, the Ouray Perimeter Trail was chosen because it provided access to study sites. The first day in Ouray consisted of traversing the entirety of the trail, a

total of 6.75 km, marking periods of extensive bark-beetle infestation on a Global Positioning System (GPS) unit for later assessment. During the assessment, an anchor point tree was chosen along the trail and 100m x 100m plots were measured from the anchor tree. At the corner of each plot, penetrometer measurements, Munsell soil colors, and types of soil were recorded. Within each plot, the amount of affected versus unaffected trees were tallied to assess the spread of the beetle within each plot. This process was repeated throughout the perimeter trail for a total of nine plots over the course of the six-day visit.

Landsat Acquisition

Following field work, remote sensing was utilized to quantitatively assess the spread of the bark-beetles over the last ten years. Landsat Ecosystem Disturbance Adaptive Processing System (LEDAPS) corrected Landsat 5 Thematic Mapper (TM) and Landsat 8 Operational Land Imager (OLI) imagery data from 2005 to 2016 was downloaded from the USGS EarthExplorer website (accessed 21 February, 2017). These scenes were chosen along the Landsat World Reference System II that contain the study area (Path 35/Row 34). The chosen images were acquired close to the middle of growing season from early July through late August with minimal cloud cover, as described by Meddens et al. (2013). The downloaded imagery was then clipped to the study extent of the Ouray USGS quadrangle, which would further expedite the process when repeated through the time series.

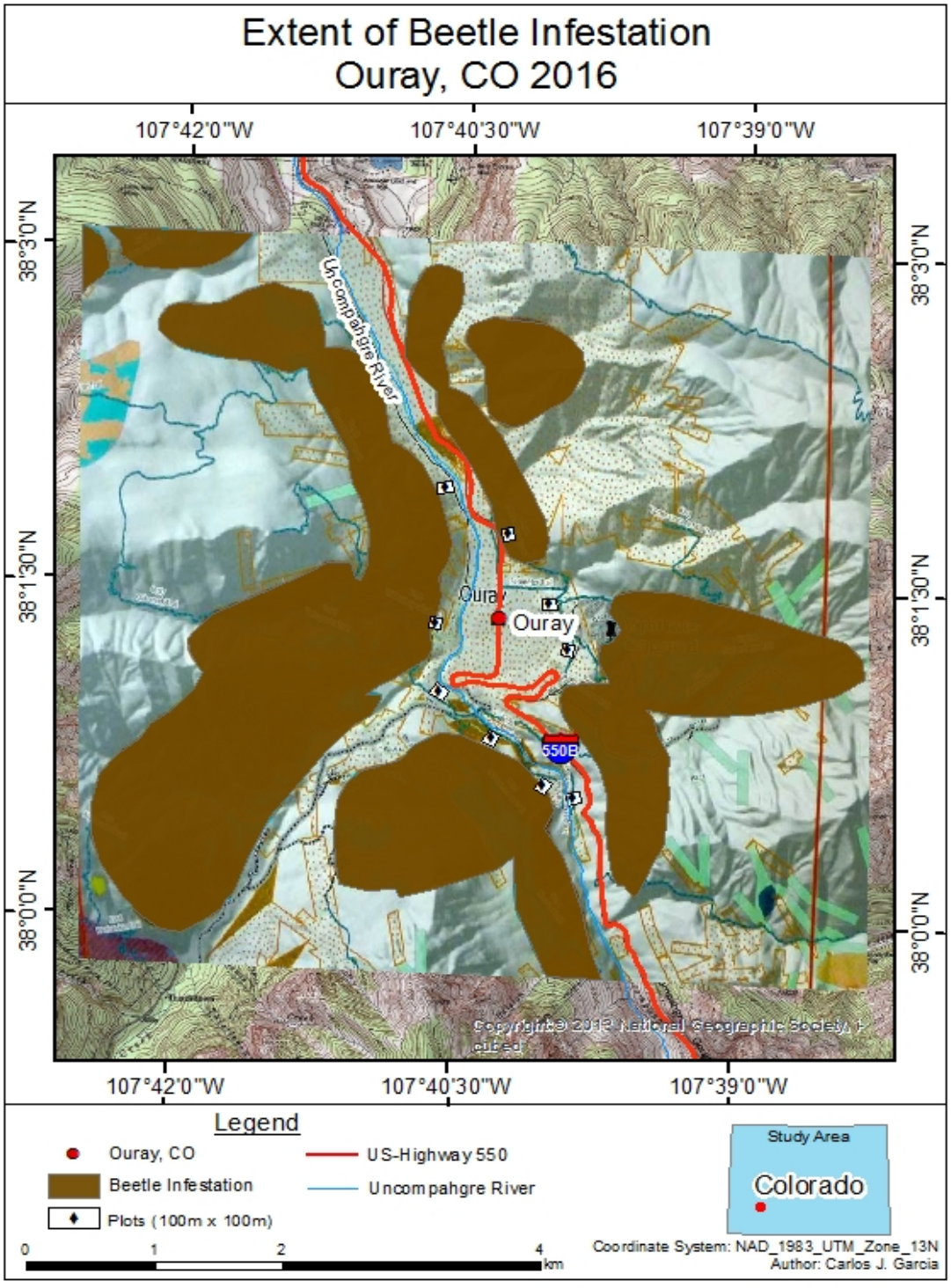

Figure 11: Extent of beetle infestation within Ouray, CO. Modified from Wright, 2016.

NDVI

NDVI is a useful vegetation index for distinguishing between gray-stage spruce beetle outbreak and non-forest in mountain pine beetle infested areas (Hart and Veblen, 2015). NDVI is a spectral index obtained from remotely sensed images in the red and near infrared portions of the spectrum (Marchetti et al., 2016). Generally, healthy vegetation will absorb most of the visible light and reflect more near-infrared light. The opposite applies of unhealthy or dying vegetation, whereas bare soils reflect in the moderate range between the two bands (Holme et al., 1987). NDVI is calculated on a per-pixel basis as the difference between near infrared and red bands, which depend on the satellite imagery being used. Band designations are summarized below along with the equation for NDVI:

Table 2: NDVI band designations by sensor with associated wavelengths.

Band	Landsat 5 (TM+)	Landsat 8 (OLI)
Red Band	Band 3 (0.63-0.69 μm)	Band 4 (0.64-0.67 μm)
Near Infrared (NIR) Band	Band 4 (0.76-0.90 μm)	Band 5 (0.85-0.88 μm)

$$NDVI = \frac{NearInfrared_{band} - Red_{band}}{NearInfrared_{band} + Red_{band}} \quad (4)$$

NDVI values range from -1 to 1, with open water correlating to negative values, and green vegetation corresponding to positive values (Marchetti et al., 2016).

Contributions from the atmosphere to NDVI are significant and can amount to 50% or more over thin or broken vegetation cover (Song et al., 2001). Because of the

different conditions through Landsat acquisition years, radiometric normalization was necessary to compare reflectances across images. This was taken into account for by utilizing the LEDAPS-corrected imagery, which processes using correction routines developed for the Terra MODIS instrument (Vermote et al, 1997). NDVI was calculated using surface reflectance (SR) bands, which is the true reflectance of Earth unaffected by clouds and other atmospheric components. This type of measurement is derived from calibrated radiance images corrected for atmospheric conditions, and allows for true interpretation of the vegetation on the surface of Earth (Shippert, 2013).

To correct for clouds and water in each scene, a mask was applied to every image in order to solely assess vegetation indices throughout the imagery. The NDVI in each image was found to be bimodal, a feature not common in vegetative NDVI values. To correct for this, clouds, bare rock, and water were identified and masked to a value of -5, well out of the scope of vegetative values. This allows for these values to be filtered out during statistical analysis to focus on flora. NDVI was calculated for each calendar year of imagery acquired before creating a time series map using the ENVI remote sensing geospatial program.

Analysis of NDVI over the time interval involved using the Raster Calculator function in ArcGIS® to calculate the mean value of each pixel. Each raster, from the years 2005 thru 2016 were used, with the exceptions of 2012 and 2015, which created a raster of mean NDVI values. The exception in 2012 was because SLC-off issues with Landsat 7 data, which caused banding of missing imagery data. After careful consideration, it was decided against using software to interpolate data because the

values would not accurately show the true environmental conditions in the area. 2015 Landsat 8 OLI imagery data contained over 90% cloud coverage within the area of interest, leaving the year unusable for analysis. This raster was then converted to points using the appropriate ArcGIS® tool and then exported as an ASCII text file, which was then imported into Microsoft Excel for further manipulation.

Once the entire time series was calculated, a final raster calculation between the first and final year within the time series was calculated to quantify the change in NDVI values from beginning to most recent.

Surface Runoff

To determine if a link exists between rates of tree mortality and rates of erosion, a classification scheme must be applied to the Landsat time series. This was done by using an unsupervised classification of NDVI values into appropriate surficial features such as exposed rock, water bodies, or vegetation. Unsupervised classification is a means by which pixels in an image are assigned to spectral classes without the user interacting with the data (Richards and Jia, 2006). This method is performed most often using clustering methods and can determine the spectral class of each pixel (Richards and Jia, 2006). Doing this gives the number of pixels that will be classified below a certain threshold of NDVI values, which can then be used to calculate surface runoff in the area and can be used to establish changes in surface compaction, which can result in increased overland flow and surface-wash erosion for different aspects and different

elevations. In this case, the unsupervised classification yielded a cutoff of 0.38 NDVI as the classification break for what will be presumed alive and dead forest vegetation.

The method formulated to quantify free water available as surface erosion is based on several assumptions because of the limitations of this project in technology and available information given. Assumptions devised include each NDVI pixel in the unsupervised classification contains full Douglas-fir and White fir tree coverage, each pixel contains only Douglas-fir and White Fir trees, water uptake is assumed to be the same for every pixel above the 0.38 NDVI threshold, which is assumed to be an alive tree, canopy reach would be the same for every tree, and each pixel has the same number of trees. This evaluation is a preliminary method for predicting surface erosional runoff.

To quantify the number of trees within the area of a pixel, individual pixel size must be divided by the canopy reach of each tree in question. White Fir and Douglas-fir trees have canopy reaches ranging from 4.6 to 6.1 meters and 6.1 to 9.1 meters, respectively (Arbor Day Foundation; Ohio State University; SelecTree). This gives an average of 6.86 meters of canopy reach per tree. The total number of trees per pixel can then be calculated by dividing pixel size by canopy reach, as seen in equation 5.

$$T_n = \frac{P_s}{C_c} \tag{5}$$

where,

T_n = Total number of trees per pixel,
P_s = Pixel size based on raster, and
C_c = Average canopy cover reach.

Values of average stand transpiration for a similar species to the White Fir, Pacific Silver Fir (*Abies amabilis)* ranged from 0.01 to 3.52 mm/day, with a stand density of 1,941 trees (Martin et al., 1997). This equates to 19.4 to 6,832,30 mm/day for an individual tree. This number is dwarfed by the transpiration rate of 2-m and 80-m for a Douglas-fir tree over a 170-day period, which was found to be 4,300,000 to 390,000,000 mm respectively (Waring and Running, 1976). These two studies were conducted in the Cascade Mountains of Washington and Oregon state, respectively (Martin et al., 1997; Waring and Running, 1976). By knowing these values for water storage for individual trees, the amount of water available as surface flow can be calculated. The amount of water available as surface flow will be calculated using equation 6 for trees with NDVI values greater-than or equal-to 0.38, as devised by the unsupervised classification. These values can be used to model the temporal and spatial rates of surface erosion based on drought and infestation spread.

$$SR = \Sigma \frac{(K\,(P_c - (T_n U)))}{T_n} \qquad (6)$$

where,

SR = Surface runoff,
K = Soil-erodibility factor derived from RUSLE equation,
P_A = Average precipitation,
T_n = Total number of trees per pixel calculated to be 131, and
U = Average amount of water used per tree.

For areas of pixels classified below the 0.38 NDVI threshold, the assumption would be that a tree would be classified as fully dead and no longer taking up water,

leaving any precipitation within its catchment zone as runoff and can be quantified as equation 7.

$$SR = \Sigma \frac{(K)\ (P_c)}{T_n} \quad (7)$$

where,

SR = Surface runoff,
K = Soil-erodibility factor derived from RUSLE equation, and
P_A = Average precipitation.

To accomplish these tasks, Raster Calculations will be done to calculate outputs for equations 6 and 7 in conjunction with the Spatial Analyst Con Tool will be used within ArcGIS®. This tool uses previously calculated unsupervised NDVI vectors in order to verify whether to apply either equation 6 to alive trees above or equal to the 0.38 NDVI threshold, or apply equation 7 to areas under the threshold.

Results

NDVI Time Series

Figure 12 shows the time series of Landsat NDVI images for the years of 2005 to 2016. This time series shows the progression of lower NDVI values through the years of study, especially between the years of 2011 – 2013. Figure 14 shows percentage of distribution of values within each range and the average value of NDVI for each pixel through the time series. This average shows a normally distributed bell curve for NDVI values, with the largest percentage of NDVI values falling within the 0.30 to 0.40 NDVI range with a mean value of 0.36 and standard deviation of 0.14.

The calculated difference between NDVI values from 2005 to 2016 were calculated by the Image Analysis tool using the difference button. The output raster, as seen in Figure 13 shows the maximum negative change in NDVI over the course of the time series was -0.53 and the maximum increase being 0.57 with a mean change of 0.08 and standard deviation of 0.09.

Surface Runoff

The application of equation 6 to the areas above or equal to the 0.38 NDVI threshold was calculated four times using the range of water uptake values found in Martin et al., 1997 Waring and Running, 1976 and applied using the Con tool in ArcGIS®. The range of values of surface runoff ranged between -390,000,000 mm to -0.2 mm per tree within each pixel with a mean value between -146,916,924 mm and -5.2 mm and standard deviation of 12.6 mm – 83,674,617 mm. This is equivalent to total precipitation available for surface runoff between -51,090,000,000 mm and -26.2 mm of within each stand in the 900 m^2 pixel.

Equation 7 was applied to calculate surface runoff in areas below the 0.38 NDVI threshold devised by the unsupervised classification using the Con tool in ArcGIS®. The resulting calculation yielded values of surface runoff ranging between 0.05 to 8.53 mm of runoff per tree classified below the threshold with a mean of 2.15 mm and a standard deviation of 1.66 mm within each 30 m x 30 m pixel (Figure 15). This equates to 6.55 - 1,117.43 mm of precipitation as surface runoff within each pixel when the individual number of trees is taken out of the equation.

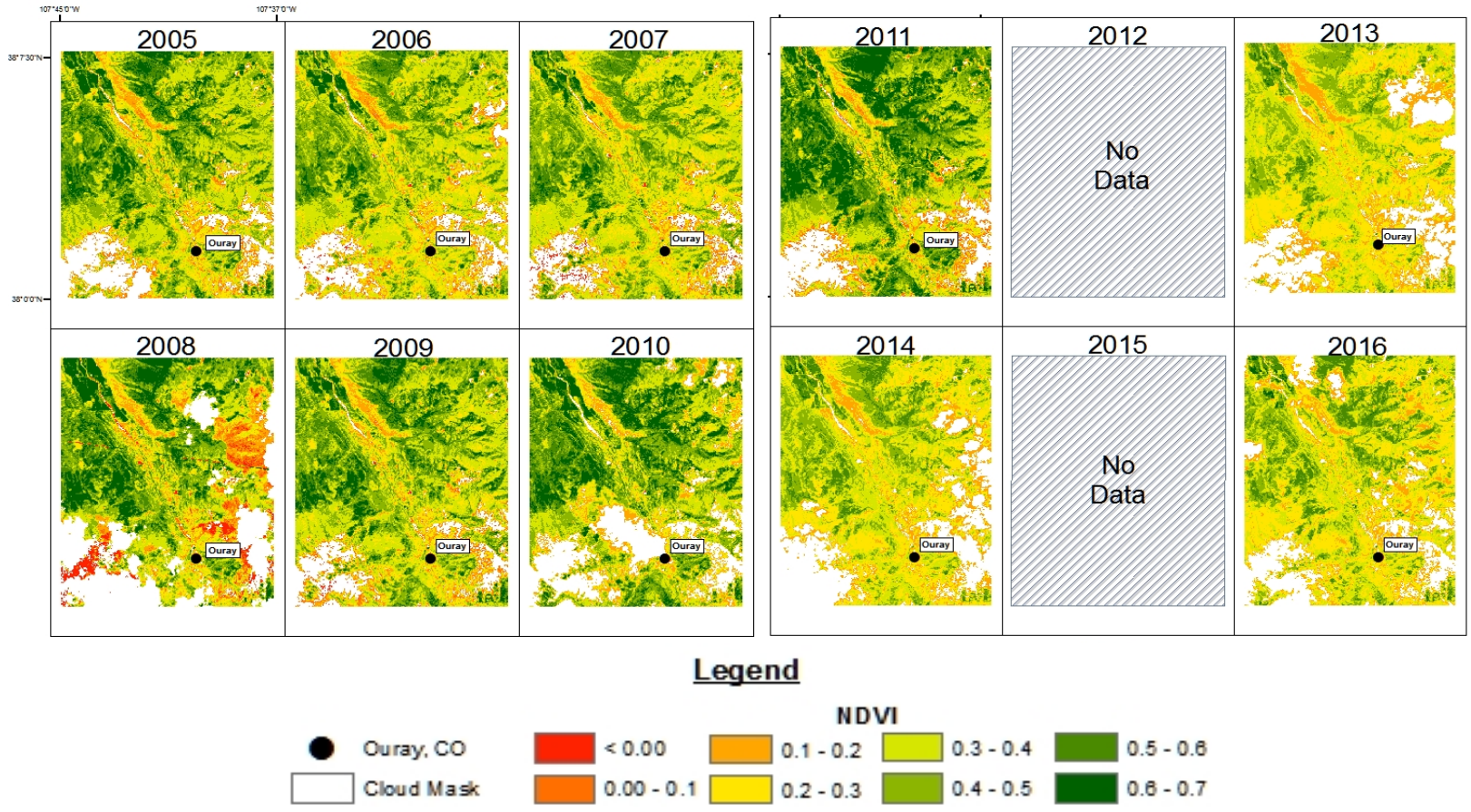

Figure 12: Time series showing change in NDVI from 2005 - 2016. Exceptions include 2012 and 2015 because of environmental and imagery limitations.

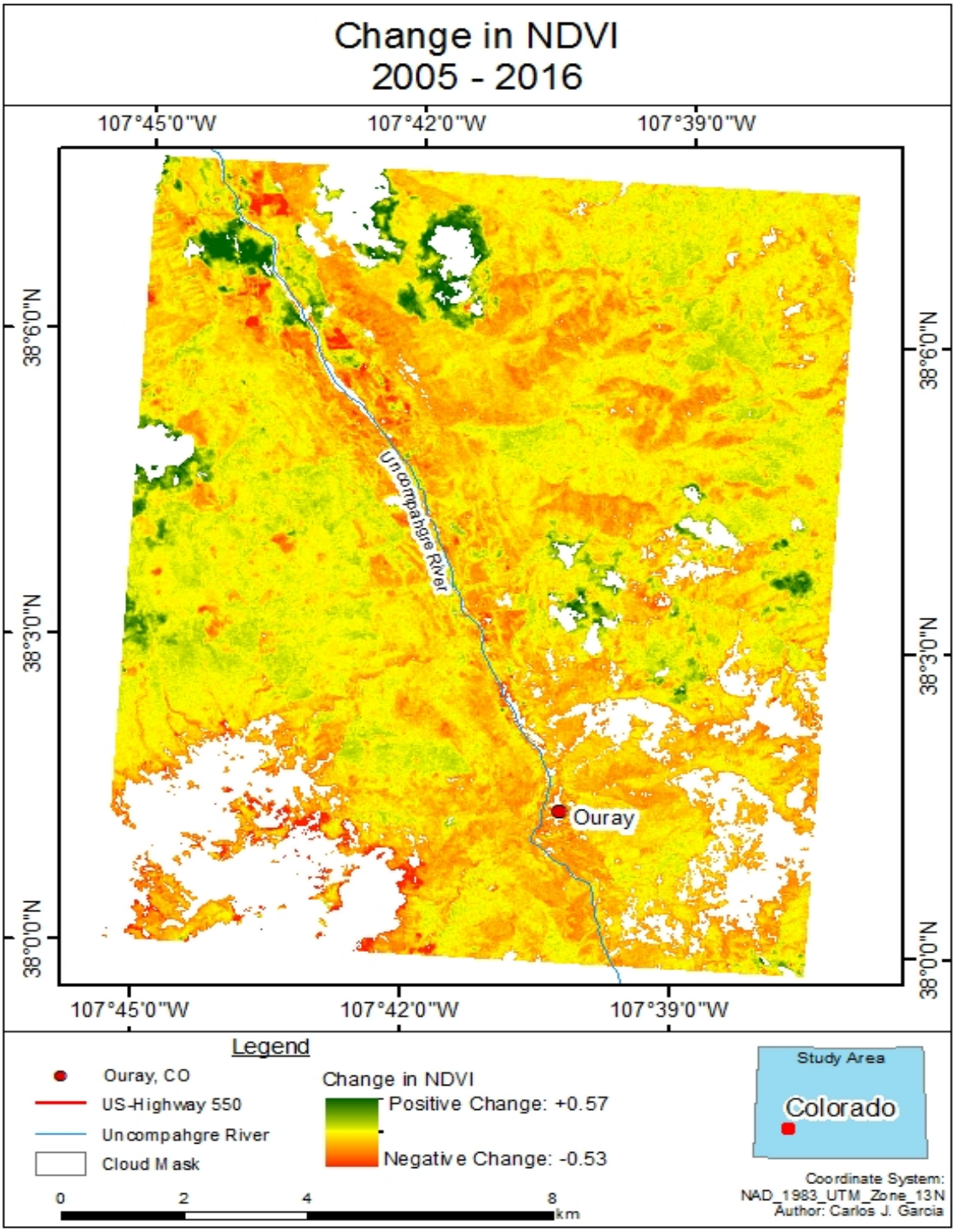

Figure 13: Calculated change in NDVI from 2005 to 2016 showing overall negative change within Ouray quadrangle.

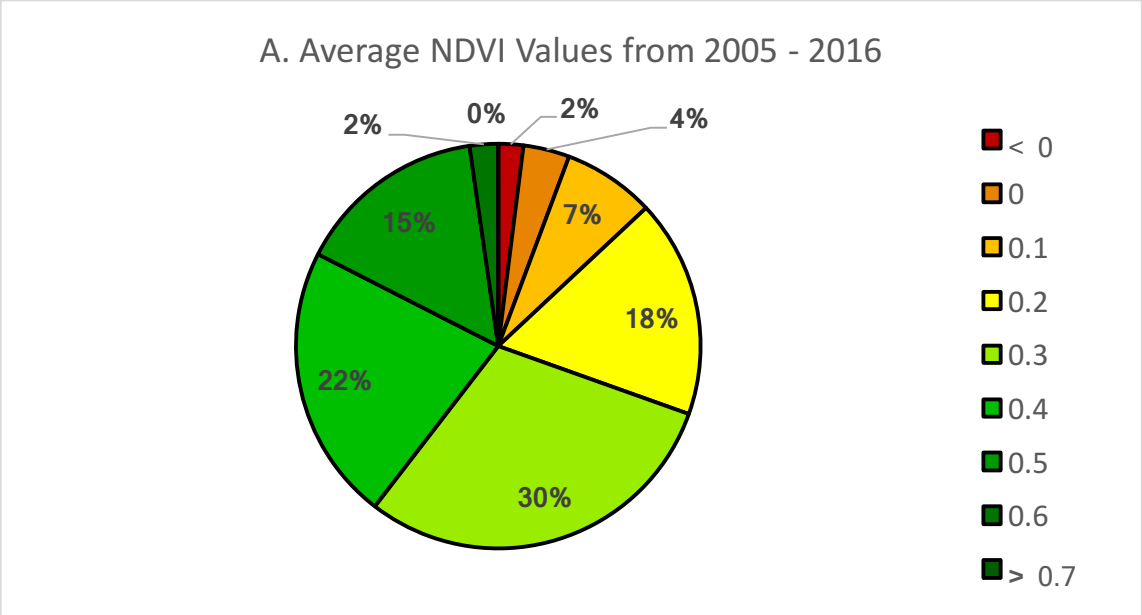

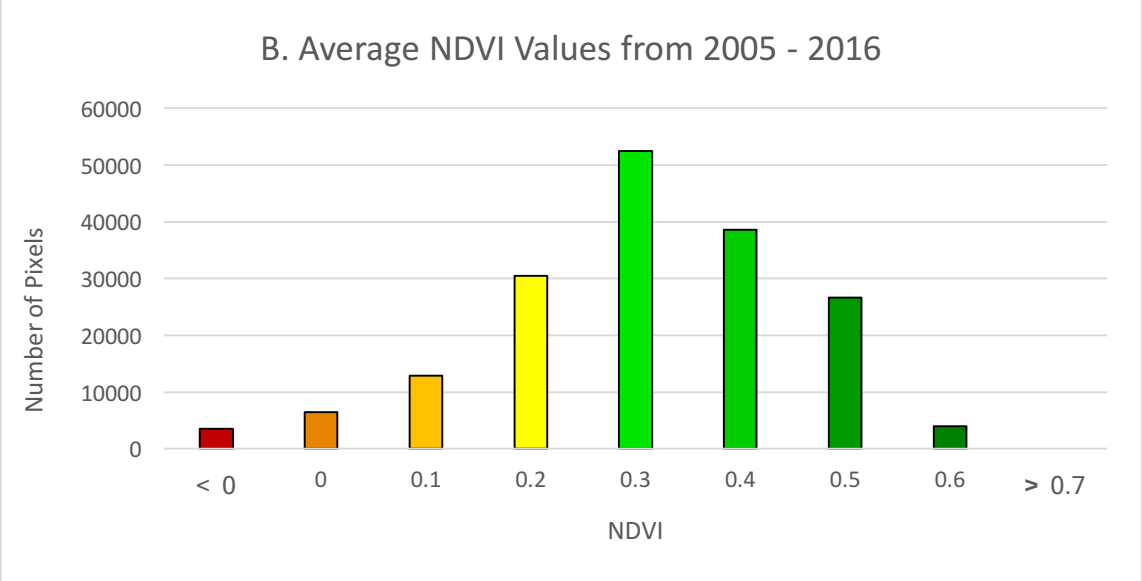

Figure 14: (A) Pie chart showing average percentage of NDVI values by category. (B) Histogram showing resemblance of bell-curve normal distribution of average time-series NDVI values.

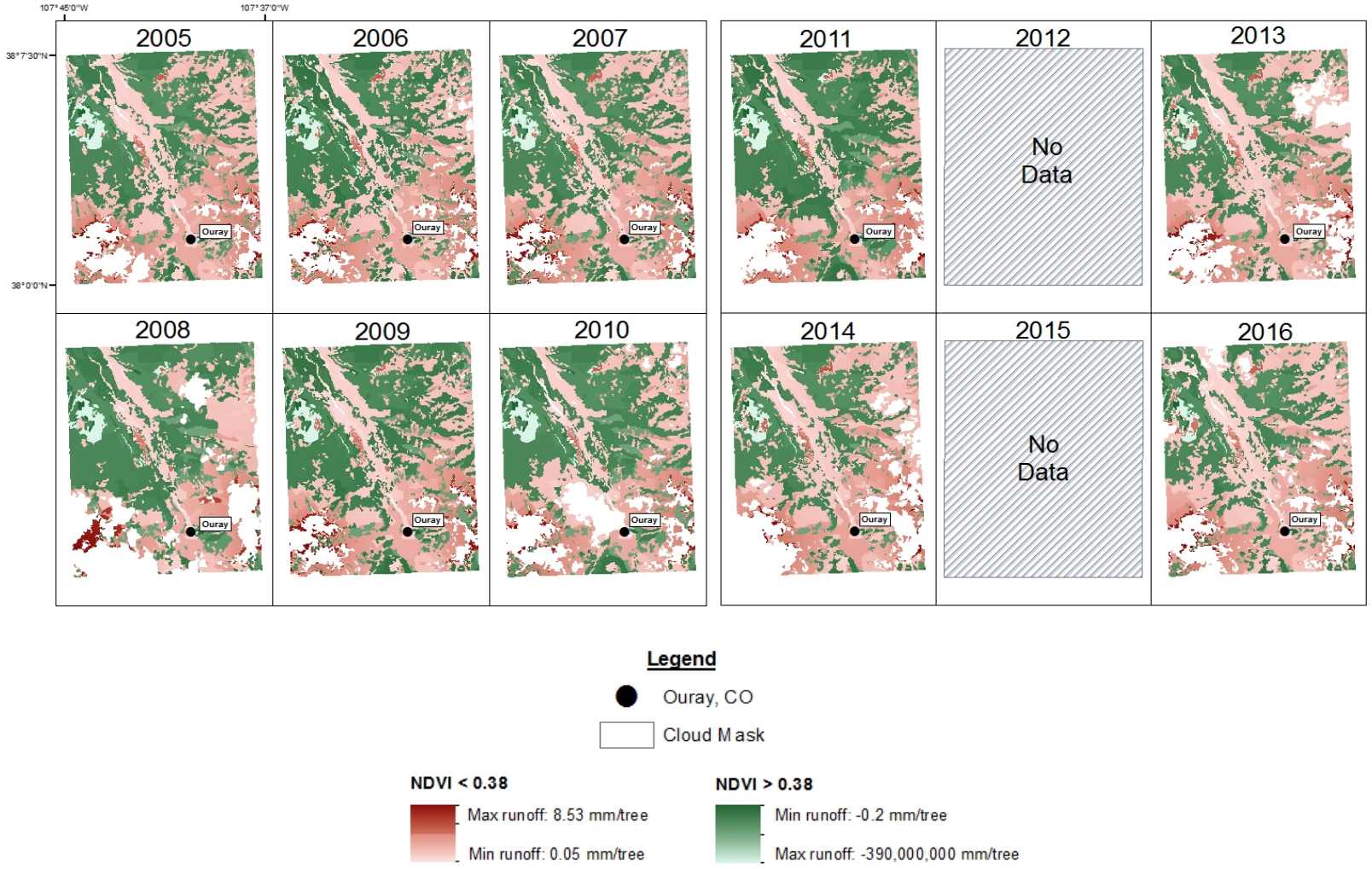

Figure 15: Time series showing surface runoff based off NDVI threshold calculated by unsupervised classification from 2005 - 2016.

Discussion

NDVI Time Series

Vegetation is extremely dynamic and can vary immensely over time and can also be affected by the time at which the Landsat image was taken, the angle of the sun on the surface, any shadows cast by clouds, NDVI values that were unable to be masked, among a number of other factors. Studies such as this can be performed at a wide variety of temporal scales to fully assess the beetle outbreak.

This study was limited by the amount and quality and quantity of remotely sensed imagery. This includes the gaps in data in the years of 2012 and 2015 because of atmospheric conditions and sensor malfunctions on Landsat 7 ETM+ as well as using different sensors as technology progressed through the time scale in this study. These factors were attempted to be mitigated by using only daytime imagery of the area during peak growing seasons. Analyzing a positively identifying change within NDVI values through the time series, and knowing through field work confirmation that forest cover has been affected by bark-beetle infestations, however, it may be supported that bark-beetle vectors grew in the time of this study, with the biggest negative change occurring from 2011 – 2013.

Statistical Analysis of NDVI Time Series

To quantify whether NDVI changed over the time series, statistical analysis had to be conducted. A chi-squared goodness of fit test was chosen to compare a normal distribution to what was observed in the imagery. The chi-squared shows how well the

distribution of sample values conforms to a normal distribution using the test procedure known as a goodness-of-fit test (Davis, 2002). My assumption with this data is that the same number of standardized values will occur in each of the normal curve intervals. The number of observation pixels actually falling into each NDVI interval is calculated, subtracted by the number I expected to find and squared, which is then divided by the expected values for each group. These values are then summed, as seen in the equation below.

Chi-Squared Goodness-of-fit test (Davis, 2002):

$$\chi^2 = \Sigma_{j=1}^{k} \frac{(O_j - E_j)^2}{E_j} \quad (8)$$

where,

χ^2 = chi-squared statistic,
O_j = number of observations withi the jth class,
E_j = number of observations expected in the jth class, and
k = number of groups.

The total number of pixel value groups was 9, giving 8 degrees of freedom for our χ^2 test. The given p-value calculated from this test equaled an unexpected value of 0.00, meaning that the data completely follows a normal distribution and the null hypothesis can be rejected, accepting the alternative hypothesis, H_A, that NDVI changed over the course of the time series. This extremely low p-value can be attributed to the extremely large number of pixels in the scene. This, coupled with the small degree of freedom, leads to the assumption that the level of significance is extremely small for this index.

Surface Runoff

The surface runoff calculation provided a first approximation on how to utilize NDVI to spatially classify and quantify surface runoff caused by bark-beetle-induced tree mortality. The extreme negative values of surface erosion are caused by the high transpiration values by Douglas-fir and Pacific Silver Fir trees. No information was available for White Fir, which led to widening the scope of research to a study on the Pacific Silver Fir (*Abies amabilis*), a type of fir within the same genus as the White Fir. This calculation was limited by the amount of literature available on Douglas-fir and White Fir trees, and no definitive consensus on rates of transpiration. This lack of consensus was to be expected, because so many different variables exist in studies ranging from the environmental conditions to the size of trees. Literature referenced was conducted in areas of extremely high annual precipitation within the Cascade Mountains of Washington and Oregon. This area is subject to the rain shadow effect, attributing to the extremely high precipitation in the area and may be an explanation as to why these studies found such high values of water uptake for both types of trees within this study (Martin et al., 1997; Waring and Running, 1976).

Future areas of improvement to this model of surface runoff include a long-term study on the types of trees within this study to establish a clear rate of transpiration that is associated with each tree in this area of Colorado coupled with field pans to measure actual surface runoff. Assumptions made during this investigation would need to be addressed, including finding higher resolution imagery to identify pixels that do not have

forest cover. This would allow for better analysis and applying this model exclusively to areas where the flora being studied is. Another possibility is using a more sophisticated method for classification. This was attempted using a parallel pipet supervised classification, but limitations in software analysis using this method resulted in large portions of the images to remain unclassified, hampering analysis.

This evaluation is a preliminary method for predicting surface erosional runoff and further study would need to be completed to diversify this model and remove these assumptions. This would make this model more representative of the true surface runoff in this study area and allow for broader application in similar environments.

Conclusions

This paper has demonstrated an accurate way to depict bark-beetle vectors through changes in NDVI using long-term remotely sensed imagery. Calculations showed maximum negative change in NDVI over the course of the time series was -0.53 and the maximum increase being 0.57 with a mean change of 0.08 and standard deviation of 0.09. The calculated p-value of the performed chi-squared test was 0.00. This means that the data completely follow a normal distribution, allowing the rejection of the null hypothesis and accept the alternative hypothesis, H_A, that NDVI changed over the course of this time series. This identified negative change in NDVI through time coupled with confirmation of trees affected by bark-beetles through field work, it may be supported that bark-beetle vectors grew in the time of this study, with the biggest negative change occurring from 2011 – 2013.

This study also provided a preliminary method for predicting surface runoff using an NDVI time series as a classification input to determine whether a tree was considered to be actively intercepting water and holding soil in place or whether the tree was no longer alive, meaning no active interception of precipitation or anchoring of soil.

Areas above the 0.38 NDVI threshold was calculated four times using the range of water uptake values giving a range of surface runoff values between -390,000,000 mm to -0.2 mm per tree within each pixel with a mean value between -146,916,924 mm and -5.2 mm and standard deviation of 12.6 mm – 83,674,617 mm. This is equivalent to total precipitation available for surface runoff between -51,090,000,000 mm and -26.2 mm of within each stand in the 900 m^2 pixel.

Surface runoff in areas below the 0.38 NDVI threshold calculated by an unsupervised classification has values of runoff ranging between 0.05 to 8.53 mm of runoff per tree with a mean of 2.15 mm and a standard deviation of 1.66 mm within each 900 m^2 pixel.

This study provides a first approximation into calculating surface runoff, which required many assumptions to be made. These extremely negative values for tree interception could be attributed to studies conducted in the Cascade Mountains, where annual precipitation is much higher than the study area in Colorado. Further study would need to be completed to diversify this surface runoff model and remove assumptions made for this preliminary study, including tree studies within this area as well as field work measuring surface runoff as a to compare model data to real world situations. This would make this model more representative of the true surface runoff in this study area

and allow for broader application in similar environments around the world. Because of these limitations, I am unable to conclude whether or not the null hypothesis can be rejected in that bark-beetle-induced tree mortality does not lead to an increase in surface runoff. Future study will allow for broader application and the ability to determine whether bark-beetle induced tree mortality leads to increased rates in surface runoff.

CHAPTER IV

DISCUSSION

Broader Impacts

Subalpine areas with trees have a high potential risk of soil erosion because of the associated extreme climatic and topographic conditions with high uncertainties in rates of erosion from spatial heterogeneity of erosion risk (Meusburger et al., 2010). This study highlights how susceptible areas such as these are to soil erosion and surface runoff and allows for these communities to plan future land use, mark areas of hazard, and devise insect mitigation tactics.

The ability to easily adjust the erosion model data to add new and updated information within GIS allows for RUSLE and surface runoff models to be used in the future using readily available data from future studies. This allows future planning within the town of Ouray, Colorado, with the ability to map areas of high soil erosion risk and hazards.

For studies involving tree and soil dynamics, this study provided a preliminary investigation for modeling soil erosion and determining surface runoff using remotely sensed data and vegetation indices. This allows subalpine areas that are susceptible to erosion and runoff the ability to analyze areas known to have higher susceptibility to mass movement as well as other environmental hazards associated with these environments.

Limitations

Studies such as this can be performed at a wide variety of temporal scales to fully assess the beetle outbreak. This study was limited by the amount and quality and quantity of remotely sensed imagery. This includes the gaps in data in the years of 2012 and 2015 because of atmospheric conditions and sensor malfunctions on Landsat 7 ETM+ as well as using different sensors as technology progressed through the time scale in this study.

This study was also severely limited by the amount of data readily available for consumption, including soil-erodibility and support practices for the entire study area. This limitation could be eliminated once published data exists for the entire study area regarding these factors, which would make the model more precise and eliminate uncertainties within these presented findings. This model was also limited in determining how much water Douglas-fir and White Fir trees intercept in precipitation, which can be addressed by further studying these trees within a long-term study.

In calculating surface runoff, a preliminary method was devised in which many assumptions were made, limiting the applicability of the model presented. Assumptions presented included limiting vegetation to Douglas-fir and White Fir trees throughout the study area, water uptake for a tree in a pixel above the threshold was assumed to be the same for every tree, which is assumed to be an alive tree, canopy reach would be the same for every tree, and each pixel has the same number of trees. Further study would need to be completed to diversify this model and remove these assumptions, which would make this model more representative of the true surface runoff in this study area.

Future Recommendations

The largest difficulty in the field work performed was how much information was actually needed. The study area was only visited one summer for seven days, and because this study was temporally based, it would be beneficial to have multi-temporal images of areas at the same time in the growing season to compare beetle propagation through time, including the regeneration of forest and its effect on erosion and runoff.

This study was limited to 2D imagery and interpretation. Future studies could include introducing updated DEM using a smaller scale or LIDAR and use advanced 3D imaging software to show this model on 3D surface.

Soil erosion and runoff calculations are also theoretical and predicted. A long-term study that would also be beneficial would be setting up markers or catchment zones for soil movement to accurately measure soil erosion and surface runoff through the duration of a beetle outbreak to further understand the beetle's role in environments such as these. This would allow the model to be adjusted to more accurately calculate the amount of erosion and runoff occurring in the area.

NDVI was the basis of this study, however, many other vegetation indices could be employed for further study and manipulation of this model, introducing further complexities for this model, bolstering its use and application. Possible indices include Greenness Above Bare Soil, Moisture Stress Index, Leaf Water Content Index, and Soil-Adjusted Vegetation Index. Further investigation into which indices is needed, but would open the door for soil, tree, and infestation dynamic modeling.

Another possibility for both models is to introduce aspect as another factor in the RUSLE calculation as well as the surface runoff calculation. This would allow analysis based on slopes facing certain directions and whether this has an effect on the slope being susceptible to soil erosion or surface runoff.

CHAPTER V

CONCLUSIONS

Introduction

Changes in forest dynamics from the recent bark-beetle infestation within Ouray, Colorado, have had a direct impact on soil erosion and subsequent runoff. Difficulties arise when coming to conclusions as to what is the dominant influence in these changing dynamics, but two main conclusions can be drawn from the data. This includes accepting the first stated alternative hypothesis, H_A, that NDVI changed over the course of the time series. Because of limitations within this study, however, I was unable to conclude whether or not the second stated null hypothesis can be rejected in that bark-beetle-induced tree mortality does not lead to an increase in surface runoff. Future study will allow for broader application and the ability to determine whether bark-beetle induced tree mortality leads to increased rates in surface runoff.

Problem Statement

This research sought to answer one main question: does a causal relationship exist between the destruction of trees by bark-beetles and increased erosion and surface runoff rates on the slopes in the Ouray, Colorado, area? After analysis of the entire area within the Ouray quadrangle within the San Juan Mountains, it is apparent that bark-beetles have had an effect on soil erosion and surface runoff. This study has shown that the change in vegetation associated during this period of bark-beetle outbreak coincide with increased values of surface runoff and soil erosion.

Objectives

Tree mortality from bark-beetles has shown to have a direct impact on slope erosion and runoff. Through this research, the following objectives were accomplished: 1. Model the rate of tree mortality and rate of erosion in the area. 2. Determine if a link exists between rate of tree mortality and rate of erosion. 3. Provide a first approximation of surface runoff and sediment production rate. These objectives were accomplished by utilizing the RUSLE equation to model rates of soil erosion, using a time series of Landsat imagery to determine the spread of tree death using NDVI, and devising a preliminary method for calculating surface runoff and applying it to areas of NDVI values below a calculated threshold.

Using various inputs in both models, including soil-erodibility, precipitation, land-cover, slope, and conservation practices, it is apparent that each of these serve a role in soil erosion and surface runoff. The question remains: does a causal relationship exists between the destruction of trees by bark-beetles and increased erosion and surface runoff rates on the slopes in the Ouray, Colorado area? Based on the analysis of data it can be concluded that NDVI was affected negatively, meaning there was a loss of vegetation cover occurred over the course of the time series study from tree mortality caused by drought-induced stress coupled with the bark-beetle infestation.

For studies involving tree and soil dynamics, this study provided a preliminary investigation for modeling soil erosion and determining surface runoff using remotely sensed data and vegetation indices. This allows subalpine areas that are susceptible to erosion and runoff the ability to analyze areas known to have higher susceptibility to

mass movement as well as other environmental hazards associated with these environments.

Summary

Soil Erosion Model

This paper has shown that the RUSLE model can effectively represent the estimation of maximum possible soil loss because of erosion within the Ouray quadrangle. R-factor was calculated to be between 0.95 – 1.15 MJ*mm/hectare*hour, and LS-Factor ranging from 0 m - 6,654.91 m. Other factors within this calculation varied spatially, with K- and C- factors between 0.01 – 1.0 and 0.00 – 1.0, respectively, depending on soil and land survey datasets.

Potential soil erosion ranges from ~0 Mg/ha/yr projected erosion in areas of low slope to a projected erosion value of ~2,3000 Mg/ha/yr in areas with extremely steep slopes and areas of high drainage output conducive to flowing water. The movement of materials down slope poses a potential hazard for the town of Ouray, Colorado, which is situated at the bottom of the valley.

Caution is needed when interpreting these results because of assumptions made to create certain parts of the model, including interpolation of soil-erodibility, K, factors. Other factors that could have affected the modeled outcome include the lack of published support practice factors for the area as well as any systemic errors within the DEM that could have attributed to errors in calculating the L and S factors, including the resampling of pixels for this calculation. With these limitations in mind and the

parameter values being reassessed, this model can be used to predict the future soil erosion within the area, which is pertinent when addressing the current beetle outbreak and subsequent erosion caused by runoff from lack of tree interception.

The results of this study have provided a first approximation and a better understanding of the quantitative changes in erosion for the Ouray quadrangle using the RUSLE equation as a model. This model offers the option to quickly identify areas of high or low rates of erosion as opposed to only utilizing rates of sediment accumulation and allows for the greater chance of determining the sources of erosion (Simms et al., 2003). This will assist in planning for any future hazards and land management within the town of Ouray and surrounding San Juan Mountains.

NDVI Time Series and Surface Runoff

This paper has demonstrated an accurate way to depict bark-beetle vectors through changes in NDVI using long-term remotely sensed imagery. Calculations showed maximum negative change in NDVI over the course of the time series was -0.53 and the maximum increase being 0.57 with a mean change of 0.08 and standard deviation of 0.09. The calculated p-value the performed chi-squared test was 0.00. This means that the data completely follows a normal distribution, allowing me to reject the null hypothesis and accept the alternative hypothesis, H_A, that NDVI changed over the course of this time series. This identified negative change in NDVI through time coupled with confirmation of trees affected by bark-beetles through field work, it may be

supported that bark-beetle vectors grew in the time of this study, with the biggest negative change occurring from 2011 – 2013.

This study also provided a preliminary method for predicting surface runoff using an NDVI time series as a classification input to determine whether a tree was considered to be actively intercepting water and holding soil in place or whether the tree was no longer alive, meaning no active interception of precipitation or anchoring of soil.

Areas above the 0.38 NDVI threshold was calculated four times using the range of water uptake values giving a range of surface runoff values between -390,000,000 mm to -0.2 mm per tree within each pixel with a mean value between -146,916,924 mm and -5.2 mm and standard deviation of 12.6 mm – 83,674,617 mm. This is equivalent to total precipitation available for surface runoff between -51,090,000,000 mm and -26.2 mm of within each stand in the 900 m^2 pixel.

Surface runoff in areas below the 0.38 NDVI threshold calculated by an unsupervised classification has values of runoff ranging between 0.05 to 8.53 mm of runoff per tree with a mean of 2.15 mm and a standard deviation of 1.66 mm within each 900 m^2 pixel. This is a first approximation into calculating surface runoff, which required many assumptions to be made.

These extremely negative values for tree interception could be attributed to studies conducted in the Cascade Mountains, where annual precipitation is much higher than the study area in Colorado. Further study would need to be completed in order to diversify this surface runoff model and remove assumptions made for this first approximation, including tree studies within this area as well as field work measuring

surface runoff as a to compare model data to real world situations. This would make this model more representative of the true surface runoff in this study area and allow for broader application in similar environments around the world.

REFERENCES

Adams, H.D., Luce, C.H., Breshears, D.D., Allen, C.D., Weiler, M., Hale, V.C., Smith, A.M.S., and Huxman, T.E., 2012. Ecohydrological consequences of drought- and infestation- triggered tree die-off: insights and hypotheses. Ecohydrology v. 5, p.145-159.

Allen, C.D., 2007. Interactions across spatial scales among forest dieback, fire, and erosion in Northern New Mexico landscapes. Ecosystems v. 10, p. 797-808.

Allen, K.K., Blodgett, J.T., Burns, K.S., Cain, R.J., Costello, S.L., Eager, T.J., Harris, J.L., Howell, B.E., Mask, R.A., Schaupp, Jr., W.C., Witcosky, J.J., and Worrall, J.J., 2010. Field Guide to Diseases and Insects of the Rocky Mountain Region. USDA Forest Service, Rocky Mountain Region, Forest Health Protection, Rocky Mountain Research Station, General Technical Report RMRS-GTR-241, p. 336.

Ammann, M., Böil, A., Rickli, C., Speck, T., and Holdenrieder, O., 2009. Significance of tree root decomposition for shallow landslides." For Snow Landsc Res., v. 82, no. 1, p. 79-94.

Anderegg, W.R.L., 2015. Tree mortality from drought, insects, and their interactions in a changing climate. New Phytologist v. 208, p. 674-683.

Arbor Day Foundation, Tree Guide – White Fir: Abies concolor. Arborday.org, https://www.arborday.org/trees/treeguide/TreeDetail.cfm?ItemID=839 (Accessed 21 April, 2017).

Bell-Randall, C., 2006. Forest Health Protection and State Forestry Organizations: Management Guide for Fir Engraver Scolytus ventralis (LeConte). US Forest Service. https://www.fs.usda.gov/Internet/FSE_DOCUMENTS/stelprdb5187436.pdf (Site visited 2 February 2017).

Bellows, T.S., Meisenbacher, C., Reardon, R.C., 1998. Biological Control of Arthropod Forest Pests of the Western United States: A Review and Recommendations, USDA FS FHTET-96-21.

Berryman, A. A., 1973. Population dynamics of the fir engraver. I. Analysis of population behavior and survival from 1964-1971. Can. Ent. v. 105, p. 1465.

Bethlahmy, N., 1974. More streamflow after a bark-beetle epidemic. Journal of Hydrology, v. 23, p. 185-189.

Biederman, J. A., et al., 2015. Recent tree die-off has little effect on streamflow in contrast to expected increases from historical studies. Water Resources Research, v. 51, no. 12, p. 9775-9789.

Bigler, C. and H. Bugmann, 2004. Predicting the time of tree death using dendrochronological data. Ecological Applications, v. 14, no. 3, p. 902-914.

Brown, M.G., Black, T.A., Nesic, Z., Fredeen, A.K., Foord, V.N., Spittlehouse, D.L., Bowler, R., Burton, P.J., Trofymow, J.A., Grant, N.J., and Lessard, D., 2012. The carbon balance of two lodgepole pine stands recovering from mountain pine beetle attack in British Columbia. Agricultural and Forest Meteorology, v. 153, p. 82–93.

Broz, B., Pfost, D., and Thompson, A., 2003. Controlling runoff and erosion at urban construction sites. University of Missouri-Columbia. http://extension.missouri.edu/explorepdf/agguides/agengin/g01509.pdf (Accessed 7 May 2017).

Burbank, W.S., and Luedke, R.G., 1981. Geology and Ore Deposits of the Uncompahgre (Ouray) Mining District, Southwestern Colorado: U.S. Geological Survey, Map I-1247, scale 1:12,000.

Burbank, W.S., and Luedke, R.G., 2008. Geology and Ore Deposits of the Uncompahgre (Ouray) Mining District, Southwestern Colorado. U.S. Geological Survey, Professional Paper 1753.

Colorado State Forest Service, 2016a. 2015 Report on the Health of Colorado's Forests 15 Years of Change. Colorado State Forest Service, Colorado State University and Colorado Department of Natural Resources.

Colorado State Forest Service, 2016b. Douglas-fir Beetle Quick Guide Series. FM 2016-1. http://csfs.colostate.edu/media/sites/22/2016/01/Douglas-Fir-Beetle-QuickGuide2016.pdf (Accessed 2 February 2017).

Colorado State Forest Service, 2016c. Fir Engraver Beetle Quick Guide Series. FM 2016-3 http://csfs.colostate.edu/media/sites/22/2016/11/Fir_Engraver_QG_1Nov_2016.pdf (Accessed 2 February 2017).

Colorado State Forest Service, 2017. 2016 Report on the Health of Colorado's Forests: Fire and Water. Colorado State Forest Service, Colorado State University and Colorado Department of Natural Resources.

Cooper, K., 2011. Evaluation of the relationship between the RUSLE R-factor and mean annual precipitation. http://www.engr.colostate.edu/~pierre/ce_old/Projects/linkfiles/Cooper%20R-factor-Final.pdf. (Accessed 20 March, 2017)

Das, G.K., Guchait, R., 2016. Modeling of risk of soil erosion in Kharkai watershed using RUSLE and TRMM data: A geospatial approach. International Journal of Science and Research v. 5, no 10.

Davis, J.C., 2002. Statistics and data analysis in geology, 3 ed. New York [u.a.]: Wiley.

Dickinson, R.G., 1988, Geologic map of the Courthouse Mountain quadrangle, Gunnison, Hinsdale, and Ouray Counties, Colorado: U.S. Geological Survey, Map GQ-1644, scale 1:24,000.

Edburg, S.L., Hicke, J.A., Lawrence, D.M., Thorton, P.E., 2011. Simulating coupled carbon and nitogen dynamics following mountain pin ebeetle outbreaks in the western United States. J. Geophys. Res.-Biogeosci., v. 116.

Edburg, S. L., Hicke, J.A., Brooks, P.D., Pendall, E.G., Ewers, B.E., Norton, U., Gochis, D., Gutman, E.D., Meddens, A.J.H., 2012. "Cascading impacts of bark-beetle-caused tree mortality on coupled biogeophysical and biogeochemical processes." Frontiers in Ecology and the Environment v, 10 no. 8, p. 416-424.

Fassnacht, F. E., Latifi, H., Ghosh, A., Joshi, P.K., and Koch, B., 2013. Assessing the potential of hyperspectral imagery to map bark-beetle-induced tree mortality. Remote Sensing of Environment, v. 140, p. 533-548.

Ferrell G.T., 1996. Fir Engraver. USDA Forest Service, Forest Insect and Disease Leaflet 13, p. 8.

Garrity, S.R, Allen, C.D., Brumby, S.P., Gangodagamage, C., McDowell, N.G., and Cai, D.M., 2013. Quantifying tree mortality in a mixed species woodland using multitemporal high spatial resolution satellite imagery. Remote Sensing of Environment v. 129, p. 54-65.

Ghimire, B., et al., 2015. "Large carbon release legacy from bark-beetle outbreaks across Western United States." Global Change Biology 21(8): 3087-3101.

Gossa, W., 2011. Soil erosion modeling using GIS and RUSLE on the Eurajoki Watershed Finland. Tampere University of Applied Sciences.

Griffin, J.M., Turner, M.G., Simard, M., 2011. Nitrogen cycling following mountain pine beetle disturbance in lodgepole pine forests of Greater Yellowstone. For. Ecol. Manage. 201 (6), 1077-1089.

Gunawan, G., Sutjiningsih, D., Soeryantono, H., and Widjanarko, S., 2013. Soil erosion prediction using GIS and remote sensing on Manjunto Watershed Bengkulu-Indonesia. Journal of Tropical Soils, v. 18 no. 2, p.141-148. doi:10.5400/jts.2013.18.2.141

Harris Geospatial Solutions, 2015. Landsat time series tutorial, https://www.harrisgeospatial.com/docs/TimeSeriesTutorial.html (accessed March 15, 2017).

Hart, S. J. and Veblen, T.T., 2015. "Detection of spruce beetle-induced tree mortality using high- and medium-resolution remotely sensed imagery." Remote Sensing of Environment v. 168 p. 134-145.

Hart, S. J., Veblen, T.T., Eisenhart, K.S., Jarvis, D., Kulakowski, D., 2014. Drought induces spruce beetle (Dendroctonus rufipennis) outbreaks across northwestern Colorado. Ecology v. 95, no. 4, p. 930-939.

Hart, S. J., Veblen, T.T., Kulakowski, D., 2014. Do tree and stand-level attributes determine susceptibility of spruce-fir forests to spruce beetle outbreaks in the early 21st century? Forest Ecology and Management, v. 318, p. 44-53.

Hicke, J.A., Johnson, M.C., Hayes, J.L., and Preisler, H.K., 2012. Effects of bark-beetle-caused tree mortality on wildfire. Forest Ecology and Management v. 271, p. 81-90.

Hicke, J.A., Meddens, A.J.H., and Kolden, C.A., 2015. Recent tree mortality in the western United States from bark-beetles and forest fires. Forest Science v. 62, no.2, p. 141-153.

Hickey, R, 2000. Slope angle and slope length solutions for GIS. Cartography, v. 29, no. 1, p. 1-8.

Holme, A.McR., Burnside, D.G., and Mitchell, A.A., 1987. The development of a system for monitoring trend in range condition in the arid shrublands of Western Australia. Australian Rangeland Journal, v. 9, p. 14-20.

Hubbard, R.M., Rhoades, C.C., Elder, K, and Negron, J., 2013. Changes in transpiration and foliage growth in lodgepole pine trees following mountain pine beetle attack and mechanical girdling. Forest Ecology and Management, v. 289, p. 312-317.

Hyde, K., Peckham, S., Holmes, T., and Ewers, B., 2016. Chapter 6 - Bark-beetle-Induced Forest Mortality in the North American Rocky Mountains A2 - Sivanpillai, R., Shroder Jr., J.F., Biological and Environmental Hazards, Risks, and Disasters. Boston, Academic Press: p. 119-135.

Kennedy, R.E., Yang, Z., and Cohen, W.B., 2010. Detecting trends in forest disturbance and recovery using yearly Landsat time series: 1. LandTrendr - Temporal segmentation algorithms. Remote Sensing of Environment v. 114, p. 2897-2910.

Kim, Y., 2014. Soil erosion assessment using GIS and Revised Universal Soil Loss Equation (RUSLE), http://www.caee.utexas.edu/prof/maidment/giswr2014/ProjectReport/Kim.pdf (accessed March 20, 2017).

Knight, J.F., Lunetta, R.L., Ediriwickrema, J., and Khorram, S., 2006. Regional Scale Land-Cover Characterization using MODIS-NDVI 250 m Multi-Temporal Imagery: A Phenology Based Approach. GIScience and Remote Sensing, v. 43, no. 1, p. 1-23.

Kurz, W.A., Dymond, C.C., Stinson, G., Rampley, G.J., Neilson, E.T., Carroll, A.L., Ebata, T., and Safranyik, L. 2008. Mountain pine beetle and forest carbon feedback to climate change. Nature, v. 452, p. 987–90.

Lausch, A., Heurich, M., Gordalla, D., Dobner, H.J., Gwillym,-Margianto, D., Salbach, C., 2013. Forecasting potential bark-beetle outbreaks based on spruce forest vitality using hyperspectral remote-sensing techniques at different scales. Forest Ecology and Management, v. 308, p. 76-89.

Macias-Samano, J.E and Borden, J.H., 2000. Interactions between Scolytus ventralis and Pityokteines elegans (Coleoptera: Scolytidae) in Abies grandis. Environmental Entomology, v. 29, no. 1, p. 28-34.

Macias-Samano, J.E., Borden, J.H., Gries, R., Pierce, Jr., H.D., Gries, G., and King, G.G.S., 1998. Primary attraction of the fir engraver, Scolytus ventralis. Journal of Chemical Ecology, v. 24, no. 6, p. 1049-1075.

Marchetti, Z.Y., Minotti, P.G., Ramonell, C.G., Schivo, F., and Kandus, P., 2016. NDVI patterns as indicator of morphodynamic activity in the middle Paraná River floodplain. Geomorphology, v. 253, p. 146-158.

Martin, T.A., Brown, K.J., Cermák, J., Ceulemans, R., Kucera, J., Meinzer, F.C., Rombold, J.S., Sprugel, D.G., and Hinckley, T.M., 1997. Crown conductance and tree and stand transpiration in a second-growth *Abies amablis* forest. Canadian Journal of Forest Research v. 27, p. 797-808.

Meddens, A.J.H., Hicke, J.A., Vierling, L.A., and Hudak, A.T., 2013. Evaluating methods to detect bark-beetle-caused tree mortality using single-date and multi-date Landsat imagery. Remote Sensing of Environment, v. 132, p. 49-58.

Meddens, A.J. H., and Hicke, J.A., 2014. Spatial and temporal patterns of Landsat-based detection of tree mortality caused by a mountain pine beetle outbreak in Colorado, USA. Forest Ecology and Management, v. 322, p. 78–88.

Meigs, G. W., Kennedy, R.E., Cohen, W.B., 2011. A Landsat time series approach to characterize bark-beetle and defoliator impacts on tree mortality and surface fuels in conifer forests. Remote Sensing of Environment v. 115, p. 3707-3718.

Meusburger, K., Konz, N., Schaub, M., Alewell, C., 2010. Soil erosion modelled with USLE and PESERA using QuickBird derived vegetation parameters in an alpine catchment. International Journal of Applied Earth Observation and Geoinformation v. 12, p. 208-215.

Mikkelson, K. M., et al., 2013. Bark-beetle infestation impacts on nutrient cycling, water quality and interdependent hydrological effects. Biogeochemistry v. 115, no. 1, p. 1-21.

Moore, G. E., 2004. Mines, mountain roads, and rocks: Geologic road logs of the Ouray area. No. 1. Ouray Historical Society.

Morgan, R.P.C., 2009. Soil erosion and conservation. John Wiley & Sons.

Natural Resources Conservation Service, United States Department of Agriculture, 2017. Custom Soil Resource Report from http://websoilsurvey.nrcs.usda.gov/app/HomePage.htm (Accessed February 15, 2017).

Ohio State University, Abies concolor – White Fir or Concolor fir (Pinaceae), plantfacts.osu.edu, http://plantfacts.osu.edu/pdf/0246-3.pdf (Accessed 21 April, 2017).

Oliveira, A.H., Aparecida da Silva, M., Silva, M.L.N., Curi, N., Neto, G.K., and França de Freitas, D.A., 2013. Chapter 4: Development of topographic factor modeling for application in soil erosion models. Soil Processes and Current Trends in Quality Assessment. InTec, 27 February, 2013. Accessed 3, May, 2017.

Olsson, P., Lindtröm, J., Eklundh, L., 2016. Near teal-time monitoring of insect induced defoliation in subalpine birch forests with MODIS and derived NDVI. Remote Sensing of Environment, v. 181, p. 42-53.

O'Loughlin, C., Ziemer, R.R., 1982. The importance of root strength and deterioration rates upon edaphic stability in steepland forests. Proceedings of I.U.F.R.O. Workshop P.1.07-00 Ecology of Subalpine Ecosystems as a Key to Management. 2-3 August 1983, Corballis, Oregon. Oregon State University, Corvallis, Oregon, p. 70-78.

Overhulser, D., 2005. Fir Engraver Beetle. Oregon Department of Forestry Forest Health Note January 2005, p. 3.

Owen, D.R., 2003. The Fir Engraver Beetle. California Department of Forestry and Fire Protection Tree Note #10, October 2003, p. 4.

Pawlik, Ł., 2013. The role of trees in the geomorphic system of forested hillslopes — A review. Earth-Science Reviews, v. 126, p.250-265.

Reed, D.E., Ewers, B.E., Pendall, E., 2014. Impact of mountain pine beetle induced mortality on forest carbon and water fluxes. Environmental Research Letters, v. 9, 12pp.

Renard, K.G., Foster, G.R., Weesies, G.A., McCool, D.K., and Yoder, D.C., 1997. Predicting soil erosion by water: a guide to conservation planning with the revised universal soil loss equation (RUSLE). USDA Agriculture Handbook No. 703, 404 pp.

Rhoades, C.C., McCutchan, J.H., Cooper, L.A., Clow, D., Detmer, T.M., Briggs, J.S., Stednick, J.D., Veblen, T.T., Ertz, R.M., Likens, G.E., Lewis, W.M., 2013. Biogeochemistry of beetle-killed forests: explaining a weak nitrate response. Proc. Natil. Acad. Sci., v. 110 no. 5, p. 1756-1760.

Richards, J.A. and Jia, X., 2006. Remote sensing digital image analysis: An introduction. Springer-Verlag, Berlin, Germany, p. 78

Ryan, S. E., Bishop, E.L., Daniels, J.M., 2014. Influence of large wood on channel morphology and sediment storage in headwater mountain streams, Fraser Experimental Forest, Colorado. Geomorphology, v. 217, p. 73-88.

Schenk, J. A., Moore, J. A., Adams, D. L., and Mahoney, R. L., 1977. A preliminary hazard rating of grand fir stands. for mortality by the fir engraver. Forest Science v. 23, no. 1, p. 103.

Schenk, J. A., Mahoney, R. L., Moore, J. A., and Adams, D. L., 1976. Understory plants as indicators of grand fir mortality because of the fir engraver. J. Entomol. Soc. Brit. Col. v. 73, no. 21.

Schmitz, R.F. and Gibson, K.E., 1996. Douglas-fir Beetle. USDA Forest Service, Forest Insect and Disease Leaflet 5, p. 1-7.

SelecTree, 1995-2017, Pseudotsuga menziesii Tree Record, http://selectree.calpoly.edu/tree-detail/pseudotsuga-menziesii (Accessed 21 April 2017).

Senf, C., Pflugmacher, D., Wulder, M.A., and Hostert, P., 2015. Characterizing spectral–temporal patterns of defoliator and bark-beetle disturbances using Landsat time series. Remote Sensing of Environment v. 170, p. 166-177.

Shippert, P., 2013. Digital number, radiance, and reflectance, http://www.harrisgeospatial.com/Home/NewsUpdates/TabId/170/ArtMID/735/ArticleID/13592/Digital-Number-Radiance-and-Reflectance.aspx (Accessed 22 March 2017).

Simard, M., Powell, E.N., Raffa, K.F., and Turner, M.G., 2012. What explains landscape patterns of tree mortality caused by bark-beetle outbreaks in Greater Yellowstone? Global Ecology and Biogeography, v. 21, p. 556-567.

Simms, A.D., Woodroffe, C.D., and Jones, B.G., 2003. Application of RUSLE for erosion management in a coastal catchment, southern NSW. International Congress on Modelling and Simulation, v. 2, p. 678-683.

Soil Survey Staff, 2016. Gridded Soil Survey Geographic (gSSURGO) Database for Colorado. United States Department of Agriculture, Natural Resources Conservation Service. Available online at https://gdg.sc.egov.usda.gov/. (Accessed 17 April 2017).

Song, C., Woodcock, C.R., Seto, K.C., Lenny, M. P., and Macomber, S.A., 2001. Classification and change detection using Landsat TM data: when and how to correct atmospheric effects? Remote Sensing of Environment, v. 75, p. 230-244.

Stevens, R. E., 1971. Fir Engraver. USDA Forest Service, Forest Pest Leaflet 13, p. 1-7.

U.S. Geological Survey, The National Map, 2009. NED products and services: The National Map, https://nationalmap.gov/elevation.html. Accessed 1 March, 2017.

Vermote, E.F., El Saleous, N., Justice, C.O., Kaufman, Y.J., Privette, J.L., Remer, L., Roger, J.C., and Tanre, D., 1997. Atmospheric correction of visible to middle-infrared EOS-MODIS data over land surfaces: Background, operational algorithm and validation. NASA Publications, Paper 31.

Wang, C., Qi, J., Moran, S., Marsett, R., 2004. Soil moisture estimation in a semiarid rangeland using ERS-2 and TM imagery. Remote Sensing of Environment, v. 90, p. 178-189.

Waring, R. H., and S. W. Running, 1976. "Water uptake, storage and transpiration by conifers: A physiological model." In Water and Plant Life, pp. 189-202. Springer Berlin Heidelberg, 1976.

Weed, A.S., Ayres, M.P., and Hicke, J.A., 2013. Consequences of climate change for biotic disturbances in North American forests. Ecological Monographs, v. 83, no. 4, p. 441-470.

Western Regional Climate Center, 2006. http://www.wrcc.dri.edu/cgi-bin/cliMAIN.pl?coridg, (Accessed 15 June 2016).

Wright, S., 2016. “Ouray’s beetle scourge (and its silver lining). San Juan Independent, http://sjindependent.org/report/ourays-beetle-scourge-and-its-silver-lining/999 (Accessed January 21, 2017).

Zhang, Q., Shao, M., Jia, X., and Wei, X., 2017. Relationship of climatic and forest factors to drought- and heat-induced tree mortality. PLoS ONE v. 12, no. 1.

Zheng, D., Rademacher, J., Chen, J., Crow, T., Bresee, M., Le Moine, J., Ryu, S-R., 2004. Estimating aboveground biomass using Landsat 7 ETM+ data across a managed landscape in northern Wisconsin, USA. Remote Sensing of Environment v. 93, no. 3, p. 402-411.

APPENDIX

Figure A-1: Photo taken on southeastern side of Ouray Perimeter trail showing mixed conifer forest with affected trees in orange-brown color.

Figure A-2: Photo taken on eastern side of Ouray Perimeter trail near Amphitheater showing affected trees in orange-brown color.

Figure A-3: Photo taken on south side of Ouray showing western portion of town with infested trees in orange-brown color.

Figure A-4: Photo taken on west side of Ouray Perimeter trail facing west showing mixed conifer forest with affected trees in orange-brown color.

Figure A-5: Photo taken on near "Look Out Point" showing mixed conifer forest in the distance with affected trees in orange-brown color.

Figure A-6: Photo taken on eastern portion of the Ouray Perimeter Trail showing two affected trees side-by-side.

Figure A-7: Photo taken on west side of Ouray Perimeter trail in a residential area showing White Fir tree infested by beetles near a residential roofline.

Table A-1 Field notes for plots 1-5.

	Point	Easting (m)	Northing (m)	Dead	Alive	Soil Penetrom.	Munsell	Soil 1	Soil 2
Plot 1	1	265610.63	4212457.74	47	61	4.25	Gray 5/1	Cryorthents	Rock Outcr
	2	265632.18	4212358.39	27	39	4.25	Gray 5/1	Cryorthents	Rock Outcr
	3	265536.00	4212357.03						
	4	265536.00	4212447.00						
Plot 2	1	266072.00	4211380.00	50	43	2.95	Gray 3/1	Scout	Typic cryochr.
	2	266095.00	4211478.00	23	34	3.5	2.5 Y 3/2	Scout	
	3	266004.00	4211496.00						
	4	265983.00	4211405.00						
Plot 3	1	266088.71	4210234.90	26	41	4.05		Rock Outcr	Cryboralfs
	2	266037.45	4210149.98	12	20	3.3		Rock Outcr	Cryboralfs
	3	266020.68	4210246.10			4.2		Rock Outcr	Cryboralfs
	4	266091.54	4210333.55			4.0		Cryorthents	Rock Outcr
Plot 4	1	265918.18	4210332.35			3.2		Cryorthents	Rock Outcr
	2	265826.65	4210375.08			3.8			
	3	265772.00	4210291.00						
	4	265856.00	4210253.00						
Plot 5	1	265059.55	4211711.50	33	42	2.15		Cryorthents	Rock Outcr
	2	265044.52	4211613.20					Cryorthents	Rock Outcr
	3	264943.00	4211619.00						
	4	264964.00	4211717.00						

Table A-2 Field notes for plots 6-9.

	Point	Easting (m)	Northing (m)	Dead	Alive	Soil Penetrom.	Munsell	Soil 1	Soil 2
Plot 6	1	265509.73	4210729.74	32	41	1.8	5YR 5/1	Cryorthents	Rock Outcr
	2	265420.72	4210775.49			4.5	5YR 5/1	Cryorthents	Rock Outcr
	3	265369.00	4210690.00						
	4	265446.00	4210652.00						
Plot 7	1	265051.87	4211020.59	51	35	4	5YR 5/1	Cryorthents	Rock Outcrop
	2	264968.19	4211081.63			3.55	5YR 5/1	Cryorthents	Rock Outcrop
	3	265017.00	4211170.00						
	4	265110.00	4211102.00						
Plot 8	1	265150.35	4212745.58	66	86	4.15	2.5YR N 5/1	Riverwash	Cryohemists
	2	265118.96	4212842.13						
	3	265017.00	4212835.00						
	4	265050.00	4212746.00						
Plot 9	1	265950.11	4211871.03	38	41	4.4	2.5Y 4/2	N/A	N/A
	2	265942.40	4211772.51						
	3	265843.00	4211768.00						
	4	265851.00	4211867.00						